On the Robustness of Semantic Segmentation Models to Adversarial Attacks

Anurag Arnab[1] Ondrej Miksik[1,2] Philip H.S. Torr[1]
[1]University of Oxford [2]Emotech Labs
{anurag.arnab, ondrej.miksik, philip.torr}@eng.ox.ac.uk

Abstract

Deep Neural Networks (DNNs) have been demonstrated to perform exceptionally well on most recognition tasks such as image classification and segmentation. However, they have also been shown to be vulnerable to adversarial examples. This phenomenon has recently attracted a lot of attention but it has not been extensively studied on multiple, large-scale datasets and complex tasks such as semantic segmentation which often require more specialised networks with additional components such as CRFs, dilated convolutions, skip-connections and multiscale processing.

In this paper, we present what to our knowledge is the first rigorous evaluation of adversarial attacks on modern semantic segmentation models, using two large-scale datasets. We analyse the effect of different network architectures, model capacity and multiscale processing, and show that many observations made on the task of classification do not always transfer to this more complex task. Furthermore, we show how mean-field inference in deep structured models and multiscale processing naturally implement recently proposed adversarial defenses. Our observations will aid future efforts in understanding and defending against adversarial examples. Moreover, in the shorter term, we show which segmentation models should currently be preferred in safety-critical applications due to their inherent robustness.

1. Introduction

Computer vision has progressed to the point where Deep Neural Network (DNN) models for most recognition tasks such as classification or segmentation have become a widely available commodity. State-of-the-art performance on various datasets has increased at an unprecedented pace, and as a result, these models are now being deployed in more and more complex systems. However, despite DNNs performing exceptionally well in absolute performance scores, they have also been shown to be vulnerable to *adversarial examples* – images which are classified incorrectly (often with high confidence), although there is only a minimal perceptual difference with correctly classified inputs [63]. This raises doubts about DNNs being used in safety-critical applications such as driverless vehicles [37] or medical diagnosis [21] since the networks could inexplicably classify a natural input incorrectly although it is almost identical to examples it has classified correctly before (Fig. 1). Moreover, it allows the possibility of malicious agents attacking systems that use neural networks [42, 55, 59, 23]. Hence, the robustness of networks perturbed by adversarial noise may be as important as the predictive accuracy on clean inputs. And if multiple models achieve comparable performance, we should always consider deploying the one which is inherently most robust to adversarial examples in (safety-critical) production settings.

This phenomenon has recently attracted a lot of attention and numerous strategies have been proposed to train DNNs to be more robust to adversarial examples [29, 43, 57, 50]. However, these defenses are not universal; they have frequently been found to be vulnerable to other types of attacks [11, 9, 10, 34] and/or come at the cost of performance penalties on clean inputs [12, 31, 50]. To the best of our knowledge, adversarial examples have not been extensively analysed beyond standard image classification models, and often on small datasets such as MNIST or CIFAR10 [50, 31, 57]. Hence, the vulnerability of modern DNNs to adversarial attacks on more complex tasks such as semantic segmentation in the context of real-world datasets covering different domains remains unclear.

In this paper, we present what to our knowledge is the first rigorous evaluation of the robustness of semantic segmentation models to adversarial attacks. We focus on semantic segmentation, since it is a significantly more complex task than image classification [5]. This has also been witnessed by the fact that state-of-the-art semantic segmentation models are typically based on standard image classification architectures [41, 62, 33], extended by additional components such as dilated convolutions [14, 69], specialised pooling [15, 71], skip-connections [47, 7], Conditional Random Fields (CRFs) [72, 1] and/or multiscale processing [15, 13] whose impact on the robustness has never been thoroughly studied.

First, we analyse the robustness of various DNN ar-

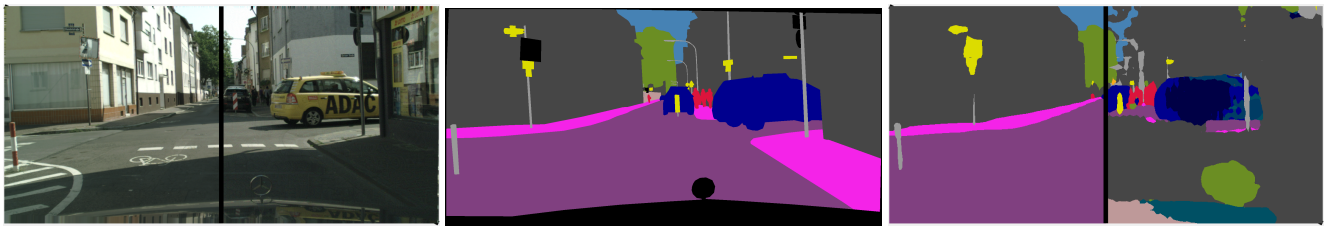

(a) Input image (perturbed half on right) (b) Ground Truth (c) PSPNet [71]

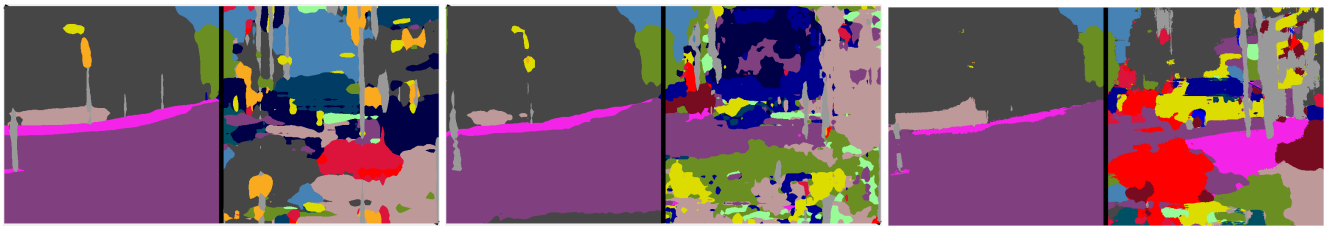

(d) DilatedNet [69] (e) ICNet [70] (f) CRF-RNN [72]

Figure 1: The left hand side shows the original image, and the right the output when modified with imperceptible adversarial perturbations. There is a large variance in how each network's performance is degraded, even though the perturbations are created individually for each network with the same ℓ_∞ norm of 4. We rigorously analyse a diverse range of state-of-the-art segmentation networks, observing how architectural properties such as residual connections, multiscale processing and CRFs all influence adversarial robustness. These observations will help future efforts to understand and defend against adversarial examples, whilst in the short term they suggest which networks should currently be preferred in safety-critical applications.

chitectures to adversarial examples and show that the Deeplab v2 network [15] is significantly more robust than approaches which achieve better prediction scores on public benchmarks [71]. Second, we show that adversarial examples are less effective when processed at different scales. Furthermore, multiscale networks are more robust to multiple different attacks and white-box attacks on them produce more transferable perturbations. Third, we show that structured prediction models have a similar effect as "gradient-masking" defense strategies [56, 57]. As such, mean field CRF inference increases robustness to untargeted adversarial attacks, but in contrast to the gradient masking defense, it also improves the network's predictive accuracy. Our fourth contribution shows that some widely accepted observations about robustness and model size or iterative attacks, which were made in the context of image classification [43, 50] do not transfer to semantic segmentation and different, real-world datasets. Finally, in contrast to the prior art [43, 46], our experiments are carried out on two large-scale, real-world datasets and (most of) our observations remain consistent across them. We believe our findings will facilitate future efforts in understanding and defending against adversarial examples without compromising predictive accuracy.

2. Adversarial Examples

Adversarial perturbations cause a neural network to change its original prediction, when added to the original input $\mathbf{x}$. For a neural network f parametrised by θ that maps $\mathbf{x} \in \mathbb{R}^m$ to y, a target class from $\mathcal{L} = \{1, 2, \ldots, L\}$, Szegedy *et al*. [63] defined an adversarial perturbation $\mathbf{r}$ as the solution to the optimisation problem

$$\arg\min \quad \|\mathbf{r}\|_2 \qquad \text{subject to} \quad f(\mathbf{x}+\mathbf{r};\theta) = y_t, \quad (1)$$

where y_t is the target label of the adversarial example $\mathbf{x}^{adv} = \mathbf{x} + \mathbf{r}$. For clarity of exposition, we consider only a single label y. This naturally generalises to the case of semantic segmentation where networks are trained with an independent cross-entropy loss at each pixel.

Constraining the neural network to output y is difficult to optimise. Hence, [63] added an additional term to the objective based on the loss function used to train the network

$$\arg\min_{\mathbf{r}} \quad c\,\|\mathbf{r}\|_2 + L(f(\mathbf{x}+\mathbf{r};\theta), y_t). \quad (2)$$

Here, L is the loss function between the network prediction and desired target, and c is a positive scalar. Szegedy *et al*. [63] solved this using L-BFGS, and [11] and [16] have proposed further advances using surrogate loss functions. However, this method is computationally very expensive as it requires several minutes to produce a single attack. Hence, the following methods are used in practice:

Fast Gradient Sign Method (FGSM) [29]. FGSM produces adversarial examples by increasing the loss (usually the cross-entropy) of the network on the input $\mathbf{x}$ as

$$\mathbf{x}^{adv} = \mathbf{x} + \epsilon \cdot \text{sign}(\nabla_{\mathbf{x}} L(f(\mathbf{x};\theta), y)). \quad (3)$$

This is a single-step, untargeted attack, which approximately minimises the ℓ_∞ norm of the perturbation bounded by the parameter ϵ.

FGSM ll [43]. This single-step attack encourages the network to classify the adversarial example as y_t by assigning

$$\mathbf{x}^{adv} = \mathbf{x} - \epsilon \cdot \text{sign}(\nabla_{\mathbf{x}} L(f(\mathbf{x}; \theta), y_t)). \quad (4)$$

We follow the convention of choosing the target class as the least likely class predicted by the network [43].

Iterative FGSM [43, 50]. This attack extends FGSM by applying it in an iterative manner, which increases the chance of fooling the original network. Using the subscript to denote the iteration number, this can be written as

$$\mathbf{x}_0^{adv} = \mathbf{x} \quad (5)$$
$$\mathbf{x}_{t+1}^{adv} = \text{clip}(\mathbf{x}_t^{adv} + \alpha \cdot \text{sign}(\nabla_{\mathbf{x}_t^{adv}} L(f(\mathbf{x}_t^{adv}; \theta), y)), \epsilon)$$

The $\text{clip}(\mathbf{a}, \epsilon)$ function makes sure that each element a_i of $\mathbf{a}$ is in the range $[a_i - \epsilon, a_i + \epsilon]$. This ensures that the max-norm constraint of each component of the perturbation $\mathbf{r}$, being no greater than ϵ is maintained. It thus corresponds to projected gradient descent [50], with step-size α, into an ℓ_∞ ball of radius ϵ around the input $\mathbf{x}$.

Iterative FGSM ll [43]. This is a stronger version of FGSM ll. This attack sets the target to be the least likely class predicted by the network, y_{ll}, in each iteration

$$\mathbf{x}_{t+1}^{adv} = \text{clip}(\mathbf{x}_t^{adv} - \alpha \cdot \text{sign}(\nabla_{\mathbf{x}_t^{adv}} L(f(\mathbf{x}_t^{adv}; \theta), y_{ll})), \epsilon). \quad (6)$$

The aforementioned attacks were all proposed in the context of image classification, but they have been adapted to the problems of semantic segmentation [26, 16], object detection [66] and visual question answering [68].

3. Adversarial Defenses and Evaluations

Liu *et al*. [46] have thoroughly evaluated the transferability of adversarial examples generated on one network and tested on another unknown model, *i.e*. only as "black-box" attacks [63, 56, 52, 53]. Kurakin *et al*. [43], contrastingly, studied the adversarial training defense, which generates adversarial examples online and adds them into the training set [29, 50, 64]. They found that training with adversarial examples generated by single-step methods conferred robustness to other single-step attacks with negligible performance difference to normally trained networks on clean inputs. However, the adversarially trained network was still as vulnerable to iterative attacks as standard models. Madry *et al*. [50], conversely, found robustness to iterative attacks by adversarial training with them. However, this was only on the small MNIST dataset. The defense was not effective on CIFAR-10, underlining the importance of testing on multiple datasets. Tramer *et al*. [64] also found that adversarially trained models were still susceptible to black-box, single-step attacks generated from other networks. Other adversarial defenses based on detecting the perturbation in the input [51, 30, 25, 67] have also all been subverted [10, 34, 9].

Currently, no effective defense to all adversarial attacks exist. This motivates us, for the first time to our knowledge, to study the properties of state-of-the-art segmentation networks and how they affect robustness to various adversarial attacks. Previous evaluations have only considered standard classification networks (Inception in [43], and GoogleNet, VGG and ResNet in [46]). We consider the more complex task of semantic segmentation, and evaluate eight different architectures, some of them with multiple classification backbones, and show that some features of semantic segmentation models (such as CRFs and multi-scale processing) naturally implement recently proposed adversarial defenses. Moreover, our evaluation is carried out on two large-scale datasets instead of only ImageNet as [43, 46]. This allows us to show that not all previously observed empirical results on classification transfer to segmentation.

The conclusions from our evaluations may thus aid future efforts to develop defenses to adversarial attacks that preserve predictive accuracy. Moreover, our results suggests which state-of-the-art models for semantic segmentation should currently be preferred in (safety-critical) settings where both accuracy and robustness are a priority.

4. Experimental Set-up

We describe the datasets, DNN models, adversarial attacks and evaluation metrics used for our evaluation in this section. Exhaustive details are included in the supplementary. We have also released our code[1] to aid reproducibility.

Datasets. We use the Pascal VOC [22] and Cityscapes [18] validation sets, the two most widely used semantic segmentation benchmarks. Pascal VOC consists of internet-images labelled with 21 different classes. The reduced validation [72, 47] set contains 346 images, and the training set has about 70000 images when combined with additional annotations from [32] and [45]. Cityscapes consists of road-scenes captured from car-mounted cameras and has 19 classes. The validation set has 500 images, and the training set totals about 23000 images. As this dataset provides high-resolution imagery (2048×1024 pixels) which require too much memory for some models, we have resized all images to 1024×512 when evaluating.

Models. We use a wide variety of current or previous state-of-the-art models, ranging from lightweight networks suitable for embedded applications to complex models

[1] www.robots.ox.ac.uk/~aarnab/adversarial_robustness.html

which explicitly enforce structural constraints. Whenever possible, we have used publicly available code or trained models. The models we had to retrain achieve similar performance to the ones trained by the original authors.

We used the public models of CRF-RNN [72], DilatedNet [69], PSPNet [71] on Cityscapes, ICNet [71] and SegNet [4]. We retrained FCN [47] and E-Net [58], as well as Deeplab v2 [15] and PSPNet for VOC as the public models are trained with the validation set. Our selection of networks are based on both VGG [62] and ResNet [33] backbones, whilst E-Net and ICNet employ custom architectures for real-time applications whose parameters measure only 1.5MB and 30.1MB in 32-bit floats, respectively. Furthermore, the models we evaluate use a variety of unique approaches including dilated convolutions [69, 15], skip-connections [47], specialised pooling [71, 15], encoder-decoder architecture [4, 58], multiscale processing [15] and CRFs [72]. In all our experiments, we evaluate the model in the same manner it was trained – CRF post-processing or multiscale ensembling is not performed unless the network incorporated CRFs [72] or multiscale averaging [15] as network layers whilst training.

Adversarial attacks. We use the FGSM, FGSM ll, Iterative FGSM and Iterative FGSM ll attacks described in Sec. 2. Following [43], we set the number of iterations of iterative attacks to $\min(\epsilon + 4, \lceil 1.25\epsilon \rceil)$ and step-size $\alpha = 1$ meaning that the value of each pixel is changed by 1 every iteration. The Iterative FGSM (untargeted) and FGSM ll (targeted) attacks are only reported in the supplementary as we observed similar trends on FGSM and Iterative FGSM ll. We evaluated these attacks when setting the ℓ_∞ norm of the perturbations ϵ to each value from $\{0.25, 0.5, 1, 2, 4, 8, 16, 32\}$. Even small values such as $\epsilon = 0.25$ introduce errors among all the models we evaluated. The maximum value of ϵ was chosen as 32 since the perturbation is conspicuous at this point. Qualitative examples of these attacks are shown in the supplementary.

Evaluation metric. The Intersection over Union (IoU) is the primary metric used in evaluating semantic segmentation [22, 18]. However, as the accuracy of each model varies, we adapt the relative metric used by [43] for image classification and measure adversarial robustness using the *IoU Ratio* – the ratio of the network's IoU on adversarial examples to that on clean images computed over the entire dataset. As the relative ranking between models for the IoU Ratio and absolute IoU is typically the same, we report the latter only in the supplementary.

5. The robustness of different architectures

We evaluate the robustness of different architectures and show how our observations regarding model capacity and single-step attacks do not corroborate with some previous findings in the context of image classification [43, 50]. Additionally, our results also support why JPEG compression as a pre-processing step mitigates small perturbations [20].

5.1. The robustness of different networks

Fig. 2 shows the robustness of several state-of-the-art models on the VOC dataset. In general, ResNet-based models not only achieve higher accuracy on clean inputs but are also more robust to adversarial inputs. This is particularly the case for the single-step FGSM attack (Fig. 2a). On the more effective Iterative FGSM ll attack, the margin between the most and least robust network is smaller as none of them perform well (Fig. 2b). However, we note that iterative attacks tend not to transfer to other models [43] (Sec. 6.2). Thus, they are less useful in practical, black-box attacks.

In particular, we have evaluated the FCN8s [47] and Deeplab-v2 with ASPP [15] models based on the popular VGG-16 [62] and ResNet-101 [33] backbones. In both cases, the ResNet variant shows greater robustness. We also observe that most of the networks achieve similar scores on clean inputs. As a result, the relative rankings of models in Fig. 2 for the IoU Ratio is about the same as their ranking on clean inputs. Furthermore, the best performing model on clean inputs, PSPNet [71] is actually less robust than Deeplab v2 with Multiscale ASPP [15]: For all ϵ values we tested, the absolute IoU score of Deeplab v2 was higher than PSPNet. These observations as well as results on FGSM ll and Iterative FGSM showing that the relative ranking of robustness for the different networks is similar, are detailed in the supplementary material.

5.2. Model capacity and residual connections

Madry *et al*. [50] and Kurakin *et al*. [43] have studied the effect of model capacity on adversarial robustness by changing the number of filters at each DNN layer, since they used the parameter count as a proxy for model capacity. Madry *et al*. [50] observed on MNIST and CIFAR-10, that networks, trained on clean examples, with a small number of parameters are the most vulnerable to adversarial examples. This observation would have serious safety implications on deployment of lightweight models, typically required by embedded platforms. Instead, we analyse different network structures and show in Fig. 3 that lightweight networks such as E-Net [58] (only 1.5 MB) and IC-Net [70] (only 30.1 MB) are affected by adversarial examples similarly as Dilated-Net [69] which has 512.6 MB in parameters (using 32-bit floats). Dilated-Net is only more robust than both of these lightweight networks for FGSM and FGSM-ll with $\epsilon \geq 4$ (which is also when perturbations become visible to the naked eye). Note that both E-Net and IC-Net have custom backbones and heavily use residual connections.

Fig. 3 also shows that adding the "Context" module of

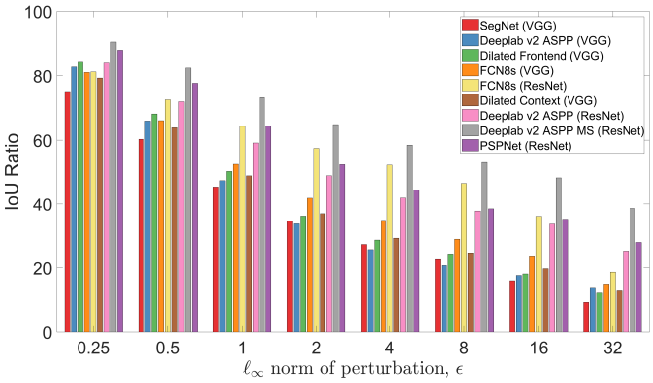

(a) Untargeted FGSM attack

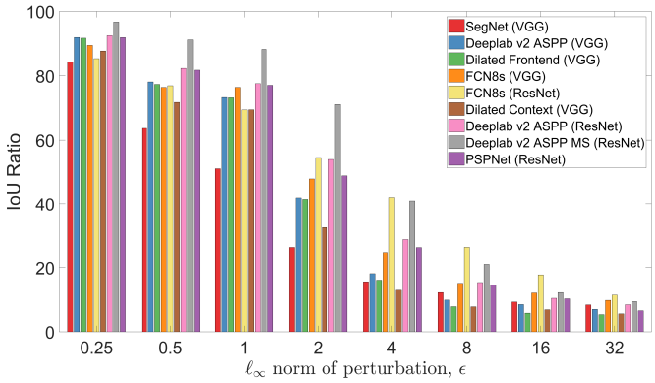

(b) Targeted Iterative FGSM ll. attack

Figure 2: Adversarial robustness of state-of-the-art models on Pascal VOC. Models based on the ResNet backbone tend to be more robust. For instance, FCN8s and Deeplab v2 ASPP with a ResNet-101 backbone are more robust than with the VGG backbone. Moreover, as expected, the Iterative FGSM ll attack is more powerful at fooling networks than single-step FGSM. Models are ordered by increasing IoU on clean inputs. Results on additional attacks are in the supplementary.

Dilated-Net onto the "Front-end" slightly reduces robustness across all ϵ values on both attacks on Cityscapes. Fig. 2 shows that this is observed for most ϵ values on VOC as well. This is even though the additional parameters of the "Context" module increases accuracy on clean inputs. Whilst models with higher capacity may be more resistant to adversarial attacks, one cannot compare the capacities of different networks, given that neither the most accurate network (PSPNet) or the network with the most parameters (Dilated-Net) are actually the most robust.

5.3. The unexpected effectiveness of single-step methods on Cityscapes

The single-step FGSM and FGSM ll attacks are significantly more effective on Cityscapes than on Pascal VOC. The IoU ratio for FGSM at $\epsilon = 32$ for PSPNet and Dilated Context is 2.5% and 2.8%, respectively, on Cityscapes. On Pascal VOC, it is substantially higher at 27.9% and 12.2%. Single-step methods (which only search in a 1-D subspace in the space of images) also appear to outperform iterative methods for high ϵ values on Cityscapes. In contrast, iterative attacks appear about as effective on Cityscapes as on Pascal VOC, when using the same hyperparameters as [43].

Thus, it may be a dataset property that causes the network to learn weights more susceptible to single-step attacks. Cityscapes has, subjectively, less variability than VOC and it also labels "stuff" classes [27]. The effect of the training set on adversarial attacks has not been considered before, and most prior work used MNIST [63, 29, 50] or ImageNet [43, 64, 46]. However, [6] and [39], showed that the test error of an SVM and neural network could respectively be increased by inserting "poisonous" examples into its training set. Results from the FGSM ll attack, which shows the same trend as FGSM, are in the supplementary.

5.4. Imperceptible perturbations

With $\epsilon = 0.25$, the perturbation is so small that the RGB values of the image pixels (assuming integers $\in [0, 255]$) are usually unchanged. Nevertheless, Fig. 2 and 3 show that the performance of all analysed models were degraded by at least 9% relative IoU for each attack. The observation of [20], that lossy JPEG as a pre-processing step helps to mitigate FGSM for small ϵ is thus not surprising as JPEG does not entirely preserve these small, high-frequency perturbations and the result is also finally rounded to integers.

5.5. Discussion

We have showed that models with residual connections (ResNet, E-Net, ICNet) are inherently more robust than chain-like VGG-based networks, even if the number of parameters of the VGG model is orders of magnitude larger. Moreover, Dilated-Net, without its "Context" module is more robust than its more performant, full version. This is contrary to the observations regarding parameter count of [50] and [43] who simply increased the number of filters at each layer. The most robust model was Deeplab v2 with Multiscale ASPP, outperforming the current state-of-the-art PSPNet [71], in absolute IoU on adversarial inputs.

We also found that perturbations that do not even change the image's integral RGB values still degraded performance of all models, and that single-step attacks are significantly more effective on Cityscapes than VOC, achieving as low as 0.8% relative IoU. This was unexpected, given that single-step methods only search in a one-dimensional subspace, and raises questions about how the training data of a network affects its decision boundaries. Also, explaining the effect of residual connections on adversarial robustness remains an open research question. As Deeplab v2 showed a significant increase in robustness over its single-scale variant, we analyse the effects of multiscale processing next in

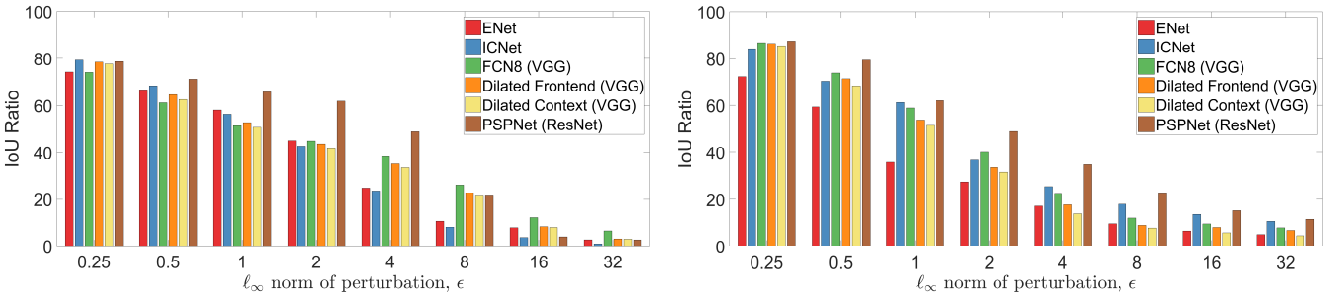

(a) Untargeted FGSM attack

(b) Targeted Iterative FGSM ll. attack

Figure 3: Adversarial robustness of state-of-the-art models on the Cityscapes dataset. Contrary to Madry *et al*. [50], we observe that lightweight networks such as E-Net [58] and ICNet [70] are often about as robust as Dilated-Net [69] ($341\times$ more parameters than E-Net). Dilated-Net without its "Context" module is slightly more robust than the full network. As with the VOC dataset, ResNet (PSPNet) architectures are more robust than VGG (Dilated-Net and FCN8). Curiously, the FGSM attack is more effective than Iterative FGSM ll which computes adversarial examples from a larger search space.

Sec. 6. Thereafter, we study CRFs, a common component in semantic segmentation models.

6. Multiscale Processing and Transferability of Adversarial Examples

Deeplab v2 with Multiscale ASPP was the most robust model to various attacks in Sec. 5, with a significant difference to its single-scale variant. In this section, we first examine the effect of multiscale processing and then relate our observations to concurrent work.

6.1. Multiscale processing

The Deeplab v2 network processes images at three different resolutions, 50%, 75% and 100% where the weights are shared among each of the scale branches. The results from each scale are upsampled to a common resolution, and then max-pooled such that the most confident prediction at each pixel from each of the scale branches is chosen [15]. This network is trained in this multiscale manner, although it is possible to perform this multiscale ensembling as a post-processing step at test-time only [14, 19, 44, 71].

We hypothesise that adversarial attacks, when generated at a single scale, are no longer as malignant when processed at another. This is because CNNs are not invariant to scale, and a range of other transformations [24, 35]. And although it is possible to generate adversarial attacks from multiple different scales of the input, these examples may not be as effective at a single scale, making networks which process images at multiple scales more robust. We investigate the transferability of adversarial perturbations generated at one scale and evaluated at another in Sec. 6.2, and the robustness and transferability of multiscale networks in Sec. 6.3. Thereafter, we relate our findings to concurrent work.

6.2. The transferability of adversarial examples at different scales

Table 1 shows results for the FGSM and Iterative FGSM ll attacks. The diagonals show "white-box" attacks where the adversarial examples are generated from the attacked network. These attacks typically result in the greatest performance degradation, as expected. The off-diagonals show the transferability of perturbations generated from other networks. In constrast to Iterative FGSM ll, FGSM attacks transfer well to other networks, which confirms the observations [43] made in the context of image classification.

The attack produced from 50% resolution inputs transfers poorly to other scales of Deeplab v2 and other architectures, and vice versa. This is seen by looking across the columns and rows of Tab. 1 respectively. All other models, FCN (VGG and ResNet) and Deeplab v2 VGG were trained at 100% resolution, and Tab. 1 shows that perturbations generated from the multiscale and 100% resolutions of Deeplab v2 transfer the best. This supports the hypothesis that adversarial attacks produced at one scale are not as effective when evaluated at another since CNNs are not scale invariant (the network activations change considerably).

6.3. Multiscale networks and adversarial examples

The multiscale version of Deeplab v2 is the most robust to white-box attacks (Tab. 1, Fig. 2) as well as perturbations generated from single-scale networks. Moreover, attacks produced from it transfer the best to other networks as well, as shown by the bolded entries. This is probably because attacks generated from this model are produced from multiple input resolutions simultaneously. For the Iterative FGSM ll attack, only the perturbations from the multiscale version of Deeplab v2 transfer well to other networks, achieving a similar IoU ratio as a white-box attack. However, this is only the case when attacking a different scale of Deeplab. Whilst perturbations from multiscale Deeplab v2 transfer better on FCN than from single-scale inputs, they are still far from the efficacy of a white-box attack (which has an IoU ratio of 15.2% on FCN-VGG and 26.4% on FCN-ResNet).

Adversarial perturbations generated from multiscale inputs to FCN8 (which has only been trained at a single scale) behave in a similar way: FCN8 with multiscale in-

Table 1: Transferability of adversarial examples generated from different scales of Deeplab v2 (columns) and evaluated on different networks (rows). The underlined diagonals for each attack show white-box attacks. Off-diagonals, show transfer (black-box) attacks. The most effective one in bold, is typically from the multiscale version of Deeplab v2.

Network evaluated	FGSM ($\epsilon = 8$)				Iterative FGSM ll ($\epsilon = 8$)			
	50%	75%	100%	Multiscale	50%	75%	100%	Multiscale
Deeplab v2 50% scale (ResNet)	<u>37.3</u>	70.5	84.8	**60.3**	<u>18.0</u>	92.0	96.9	**20.0**
Deeplab v2 75% scale (ResNet)	85.5	<u>39.7</u>	62.2	**50.8**	99.5	<u>17.9</u>	89.9	**20.4**
Deeplab v2 100% scale (ResNet)	93.6	57.9	<u>37.7</u>	**37.2**	100.0	79.0	<u>15.5</u>	**16.8**
Deeplab v2 Multiscale (ResNet)	83.7	**57.6**	62.3	<u>53.1</u>	99.6	**90.2**	91.9	<u>21.5</u>
Deeplab v2 100% scale (VGG)	94.3	70.6	66.9	**66.5**	98.9	88.4	86.3	**80.9**
FCN8 (VGG)	94.7	67.2	65.8	**65.4**	98.4	85.2	84.9	**78.5**
FCN8 (ResNet)	94.0	66.3	63.5	**63.1**	99.4	82.6	80.3	**74.1**

puts is more robust to white-box attacks, and its perturbations transfer better to other networks. This suggests that the observations seen in Tab. 1 are not properties of training the network, but rather the fact that CNNs are not scale invariant. Furthermore, an alternative to max-pooling the predictions at each scale is to average them. Average-pooling produces similar results to max-pooling. Details of these experiments, along with results using different attacks and l_∞ norms (ϵ values), are presented in the supplementary.

6.4. Transformations of adversarial examples

Adversarial examples do not transfer well across different scales and transformations, as noted by Lu *et al*. [48]. The authors created adversarial traffic signs after capturing images of them from 0.5m and 1.5m away. Whilst the printed image taken from 0.5m fooled an object detector viewing the image from 0.5m, it did not when viewed from 1.5m and vice versa. This result is corroborated by Tab.1 which shows adversarial examples transfer poorly across different scales. As CNNs are not invariant to many classes of transformations (including scale) [24], adversarial examples undergoing them will not be as malicious since the activations of the network change greatly compared to the original input. Whilst we have shown that networks are more vulnerable to black-box perturbations generated from multiple scales, there may be other transformations which are even more difficult to model for the attacks. This effectively makes it more challenging to produce physical adversarial examples in the real world [49] which can be processed from a wide range of viewpoints and camera distortions.

6.5. Relation to other defenses

Our observations relate to the "random resizing" defense of [65] in concurrent work. Here, the input image is randomly resized and then classified. This defense exploits (but does not attribute its efficacy to) the fact that CNNs are not scale invariant and that adversarial examples were only generated at the original scale. We hypothesise that this defense could be defeated by creating adversarial attacks from multiple scales, as done in this work and concurrently in [3].

7. Effect of CRFs on Adversarial Robustness

Conditional Random Fields (CRFs) are commonly used in semantic segmentation to enforce structural constraints [2]. The most common formulation is DenseCRF [40], which encourages nearby (in terms of position or appearance) pixels to take on the same label and hence prefers smooth labelling. This is done by a pairwise potential function, defined between each pair of pixels, which takes the form of a weighted sum of a bilateral and Gaussian filter.

Intuitively, one may observe that adversarial perturbations typically appear as a high-frequency noise, and thus the pairwise terms of DenseCRF which act as a low-pass filter, may provide resistance to adversarial examples. To verify this hypothesis, we consider CRF-RNN [72]. This approach formulates mean-field inference of DenseCRF as an RNN which is appended to the FCN8s network [47], enabling end-to-end training. We also report in the supplementary material similar results for DeepLab v2, which performs mean-field inference as a post-processing step.

7.1. CRFs confer robustness to untargeted attacks

Fig. 4a shows that CRF-RNN is markedly more robust than FCN8s to the untargeted FGSM and Iterative FGSM attacks. To verify the hypothesis that the smoothing effect of the pairwise terms increases the robustness to adversarial attacks, we evaluated various values of the bandwidth hyperparameters defining the pairwise potentials (not learned; in Fig. 4a, we used the values of the public model).

Higher bandwidth values (increasing smoothness) do not actually lead to greater robustness. Instead, we observed a correlation between the final confidence of the predictions (from different hyperparameter settings) and robustness to adversarial examples. We measured confidence according to the probability of the highest-scoring label at each pixel, as well as the entropy of the marginal distribution over all labels at each pixel. The mean confidence and entropy for CRF-RNN (with original hyperparameters) is 99.1% and 0.025 nats respectively, whilst it is 95.2% and 0.13 nats for FCN8s (additional details in supplementary). The fact that

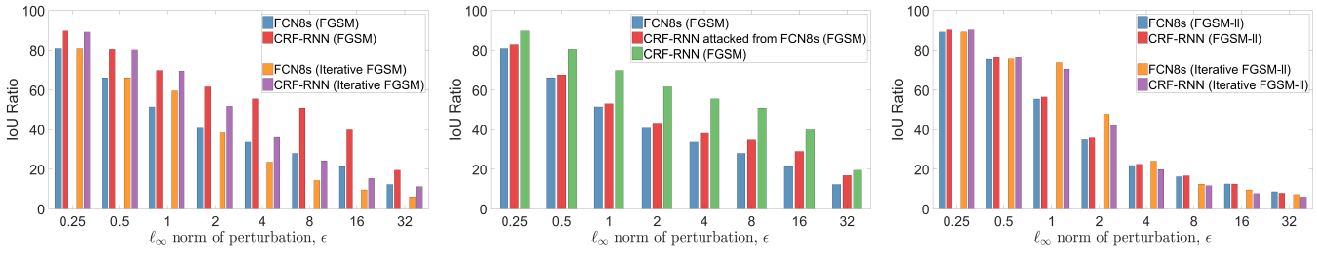

(a) (b) (c)

Figure 4: (a) On untargetted attacks on Pascal VOC, CRF-RNN is noticably more robust than FCN8s. (b) CRF-RNN is more vulnerable to black-box attacks from FCN8, due to its "gradient masking" effect which results in ineffective white-box attacks. (c) However, the CRF does not "mask" the gradient for targeted attacks and it is no more robust than FCN8s.

mean-field inference tends to produce overconfident predictions has also been noted previously by [54] and [8].

More confident predictions lead to a smaller loss, making attacks which use the gradient of the loss with respect to the input less effective. The "Defensive Distillation" approach of [57] made use of a similar fact by increasing the confidence of the model's predictions, resulting in gradients of smaller norm. The key difference is that CRFs increase the confidence as a by-product of a technique generally used to improve accuracy on numerous pixel-wise labelling tasks, while the effect of [57] on accuracy is unknown, as it was only tested on the saturated MNIST and CIFAR10 datasets.

7.2. Circumventing the CRF

Although CRFs are more resistant to untargeted attacks, they can still be subverted in two ways. CRF-RNN is effectively FCN8s with an appended mean-field layer. Fig. 4b shows, that adversarial examples generated via FGSM from FCN8s ("unary" potentials) are more effective on CRF-RNN than attacks from the output layer of CRF-RNN.

Also, targeted attacks with FGSM ll and Iterative FGSM ll are more effective since the label used to compute the loss for generating the adversarial example is not the network's (highly confident) prediction but rather the least likely label. Consequently, the loss is high and there is a strong gradient signal from which to compute the adversarial example. Fig. 4c shows that CRF-RNN and FCN8s barely differ in their adversarial robustness to targeted attacks.

7.3. Discussion

The smoothing effect of CRFs, perhaps counter-intuitively, has no impact on the adversarial robustness of a DNN. However, mean-field inference produces confident marginals, making untargeted attacks less effective since they rely on the gradient of the final loss with respect to the prediction. Black-box attacks generated from models without a CRF transfer well to networks with a CRF, and are actually more effective. This is the case for both CRFs trained end-to-end [72] and used as post-processing [15], as shown in the supplementary. Finally, CRFs confer no robustness to untargeted attacks. Our investigation of the CRF also underlines the importance of testing thoroughly with black-box attacks and multiple attack algorithms, which is not the case for numerous proposed defenses [17, 28, 29, 57].

8. Conclusion

We have presented what to our knowledge is the first rigorous evaluation of the robustness of semantic segmentation models to adversarial attacks. We believe our main observations will facilitate future efforts to understand and defend against these attacks without compromising accuracy:

Networks with *residual connections* are inherently more robust than chain-like networks. This extends to the case of models with very few parameters, contrary to the prior observations of [43, 50]. *Multiscale* processing makes CNNs more robust since adversarial inputs are not as malignant when processed at a different scale from which they were generated at, probably as CNNs are not invariant to scale. The fact that CNNs are not invariant to many classes of transformations also makes producing physical adversarial attacks more difficult. Note, however, that multiscale perturbations also transfer better to other models. *Mean-field inference for Dense CRFs*, which increases the confidence of predictions confers robustness to untargeted attacks, as it naturally performs "gradient masking" [56, 57].

In the shorter term, our observations suggest that networks such as Deeplab v2, which is based on ResNet and performs multiscale processing, should be preferred in safety-critical applications due to their inherent robustness. As the most accurate network on clean inputs is not necessarily the most robust network, we recommend evaluating robustness to a variety of adversarial attacks as done in this paper to find the best combination of accuracy and robustness before deploying models in practice.

Adversarial attacks are arguably the greatest challenge affecting DNNs. The recent interest into this phenomenon is only the start of an important longer-term effort, and we should also study the influence of other factors such as training regimes and attacks tailored to evaluation metrics. In this paper, we have made numerous observations and raised questions that will aid future work in understanding adversarial examples and developing more effective defenses.

We thank Qizhu Li and Bernardino Romera-Paredes for valuable input. This work was supported by the EPSRC, Clarendon Fund, ERC grant ERC-2012-AdG 321162-HELIOS, EPSRC grant Seebibyte EP/M013774/1 and EPSRC/MURI grant EP/N019474/1.

References

[1] A. Arnab, S. Jayasumana, S. Zheng, and P. H. S. Torr. Higher order conditional random fields in deep neural networks. In *ECCV*, 2016. 1

[2] A. Arnab, S. Zheng, S. Jayasumana, B. Romera-Paredes, M. Larsson, A. Kirillov, B. Savchynskyy, C. Rother, F. Kahl, and P. H. S. Torr. Conditional random fields meet deep neural networks for semantic segmentation: Combining probabilistic graphical models with deep learning for structured prediction. *IEEE Signal Processing Magazine*, 35(1):37–52, 2018. 7

[3] A. Athalye and I. Sutskever. Synthesizing robust adversarial examples. In *arXiv preprint arXiv:1707.07397v1*, 2017. 7

[4] V. Badrinarayanan, A. Handa, and R. Cipolla. Segnet: A deep convolutional encoder-decoder architecture for robust semantic pixel-wise labelling. *CoRR*, abs/1505.07293, 2015. 4, 11, 12

[5] H. G. Barrow and J. Tenenbaum. Interpreting line drawings as three-dimensional surfaces, 1981. 1

[6] B. Biggio, B. Nelson, and P. Laskov. Poisoning attacks against support vector machines. In *ICML*, 2012. 5

[7] P. Bilinski and V. Prisacariu. Dense Decoder Shortcut Connections for Single-Pass Semantic Segmentation. In *CVPR*, 2018. 1

[8] P. Carbonetto and N. D. Freitas. Conditional mean field. In *NIPS*, 2007. 8

[9] N. Carlini and D. Wagner. Defensive distillation is not robust to adversarial examples. In *arXiv preprint arXiv:1607.04311v1*, 2016. 1, 3

[10] N. Carlini and D. Wagner. Adversarial examples are not easily detected: Bypassing ten detection methods. In *arXiv preprint arXiv:1705.07263v1*, 2017. 1, 3

[11] N. Carlini and D. Wagner. Towards evaluating the robustness of neural networks. In *IEEE Symposium on Security and Privacy*, 2017. 1, 2

[12] K. Chalupka, P. Perona, and F. Eberhardt. Visual causal feature learning. In *UAI*, 2015. 1

[13] S. Chandra and I. Kokkinos. Fast, exact and multi-scale inference for semantic image segmentation with deep gaussian crfs. In *ECCV*, 2016. 1

[14] L.-C. Chen, G. Papandreou, I. Kokkinos, K. Murphy, and A. L. Yuille. Semantic image segmentation with deep convolutional nets and fully connected crfs. *ICLR*, 2015. 1, 6

[15] L.-C. Chen, G. Papandreou, I. Kokkinos, K. Murphy, and A. L. Yuille. Deeplab: Semantic image segmentation with deep convolutional nets, atrous convolution, and fully connected crfs. *arXiv preprint arXiv:1606.00915v2*, 2016. 1, 2, 4, 6, 8, 11, 12, 15, 25

[16] M. Cisse, Y. Adi, N. Neverova, and J. Keshet. Houdini: Fooling deep structured prediction models. In *NIPS*, 2017. 2, 3

[17] M. Cisse, P. Bojanowski, E. Grave, Y. Dauphin, and N. Usunier. Parseval networks: Improving robustness to adversarial examples. In *ICML*, 2017. 8

[18] M. Cordts, M. Omran, S. Ramos, T. Rehfeld, M. Enzweiler, R. Benenson, U. Franke, S. Roth, and B. Schiele. The cityscapes dataset for semantic urban scene understanding. In *CVPR*, 2016. 3, 4

[19] J. Dai, K. He, and J. Sun. Boxsup: Exploiting bounding boxes to supervise convolutional networks for semantic segmentation. In *ICCV*, 2015. 6

[20] G. K. Dziugaite, Z. Ghahramani, and D. M. Roy. A study of the effect of jpg compression on adversarial images. In *arXiv preprint arXiv:1608.00853v1*, 2016. 4, 5

[21] A. Esteva, B. Kuprel, R. A. Novoa, J. Ko, S. M. Swetter, H. M. Blau, and S. Thrun. Dermatologist-level classification of skin cancer with deep neural networks. *Nature*, 2017. 1

[22] M. Everingham, L. Van Gool, C. K. Williams, J. Winn, and A. Zisserman. The pascal visual object classes (voc) challenge. *IJCV*, 2010. 3, 4

[23] I. Evtimov, K. Eykholt, E. Fernandes, T. Kohno, B. Li, A. Prakash, A. Rahmati, and D. Song. Robust physical-world attacks on machine learning models. In *arXiv preprint arXiv:1707.08945v3*, 2017. 1

[24] A. Fawzi and P. Frossard. Manitest: Are classifiers really invariant? In *BMVC*, 2015. 6, 7

[25] R. Feinman, R. R. Curtin, S. Shintre, and A. B. Gardner. Detecting adversarial samples from artifacts. In *arXiv preprint arXiv:1703.00410v2*, 2017. 3

[26] V. Fischer, M. C. Kumar, J. H. Metzen, and T. Brox. Adversarial examples for semantic image segmentation. In *ICLR Workshop*, 2017. 3

[27] D. A. Forsyth, J. Malik, M. M. Fleck, H. Greenspan, T. Leung, S. Belongie, C. Carson, and C. Bregler. *Finding pictures of objects in large collections of images*. Springer, 1996. 5

[28] J. Gao, B. Wang, and Y. Qi. Deepmask: Masking dnn models for robustness against adversarial samples. In *ICLR Workshop*, 2017. 8

[29] I. J. Goodfellow, J. Shlens, and C. Szegedy. Explaining and harnessing adversarial examples. In *ICLR*, 2015. 1, 2, 3, 5, 8

[30] K. Grosse, P. Manoharan, N. Papernot, M. Backes, and P. McDaniel. On the (statistical) detection of adversarial examples. In *arXiv preprint arXiv:1702.06280v1*, 2017. 3

[31] S. Gu and L. Rigazio. Towards deep neural network architectures robust to adversarial examples. In *ICLR Workshop*, 2015. 1

[32] B. Hariharan, P. Arbeláez, L. Bourdev, S. Maji, and J. Malik. Semantic contours from inverse detectors. In *ICCV*, 2011. 3, 11

[33] K. He, X. Zhang, S. Ren, and J. Sun. Deep residual learning for image recognition. In *CVPR*, 2016. 1, 4

[34] W. He, J. Wei, X. Chen, N. Carlini, and D. Song. Adversarial example defenses: Ensembles of weak defenses are not strong. In *arXiv preprint arXiv:1706.04701v1*, 2017. 1, 3

[35] J. F. Henriques and A. Vedaldi. Warped convolutions: Efficient invariance to spatial transformations. In *ICML*, 2017. 6

[36] J. Huang, V. Rathod, C. Sun, M. Zhu, A. Korattikara, A. Fathi, I. Fischer, Z. Wojna, Y. Song, S. Guadarrama, et al. Speed/accuracy trade-offs for modern convolutional object detectors. In *CVPR*, 2017. 12

[37] J. Janai, F. Güney, A. Behl, and A. Geiger. Computer vision for autonomous vehicles: Problems, datasets and state-of-the-art. In *arXiv preprint arXiv:1704.05519v1*, 2017. 1

[38] Y. Jia, E. Shelhamer, J. Donahue, S. Karayev, J. Long, R. Girshick, S. Guadarrama, and T. Darrell. Caffe: Convolutional architecture for fast feature embedding. *arXiv preprint arXiv:1408.5093*, 2014. 11

[39] P. W. Koh and P. Liang. Understanding black-box predictions via influence functions. In *ICML*, 2017. 5

[40] P. Krähenbühl and V. Koltun. Efficient inference in fully connected CRFs with Gaussian edge potentials. In *NIPS*, 2011. 7, 25

[41] A. Krizhevsky, I. Sutskever, and G. E. Hinton. Imagenet classification with deep convolutional neural networks. In *NIPS*. 2012. 1

[42] A. Kurakin, I. Goodfellow, and S. Bengio. Adversarial examples in the physical world. In *ICLR Workshop*, 2017. 1

[43] A. Kurakin, I. Goodfellow, and S. Bengio. Adversarial machine learning at scale. In *ICLR*, 2017. 1, 2, 3, 4, 5, 6, 8

[44] G. Lin, C. Shen, and I. Reid. Efficient piecewise training of deep structured models for semantic segmentation. In *CVPR*, 2016. 6

[45] T.-Y. Lin, M. Maire, S. Belongie, J. Hays, P. Perona, D. Ramanan, P. Dollár, and C. L. Zitnick. Microsoft coco: Common objects in context. In *ECCV*. 2014. 3, 11

[46] Y. Liu, X. Chen, C. Liu, and D. Song. Delving into transferable adversarial examples and black-box attacks. In *ICLR*, 2017. 2, 3, 5

[47] J. Long, E. Shelhamer, and T. Darrell. Fully convolutional networks for semantic segmentation. In *CVPR*, 2015. 1, 3, 4, 7, 11, 12

[48] J. Lu, H. Sibai, E. Fabry, and D. Forsyth. No need to worry about adversarial examples in object detection in autonomous vehicles. In *CVPR Workshop*, 2017. 7

[49] J. Lu, H. Sibai, E. Fabry, and D. Forsyth. Standard detectors aren't (currently) fooled by physical adversarial stop signs. In *arXiv preprint arXiv:1710.03337v1*, 2017. 7

[50] A. Madry, A. Makelov, L. Schmidt, D. Tsipras, and A. Vladu. Towards deep learning models resistant to adversarial attacks. In *ICLR*, 2018. 1, 2, 3, 4, 5, 6, 8

[51] J. H. Metzen, T. Genewein, V. Fischer, and B. Bischoff. On detecting adversarial perturbations. In *ICLR*, 2017. 3

[52] J. H. Metzen, M. C. Kumar, T. Brox, and V. Fischer. Universal adversarial perturbations against semantic image segmentation. In *ICCV*, 2017. 3

[53] S.-M. Moosavi-Dezfooli, A. Fawzi, O. Fawzi, and P. Frossard. Universal adversarial perturbations. In *CVPR*, 2017. 3

[54] K. P. Murphy. *Machine learning: a probabilistic perspective*. MIT press, 2012. 8

[55] N. Papernot, P. McDaniel, and I. Goodfellow. Transferability in machine learning: from phenomena to black-box attacks using adversarial samples. In *arXiv preprint arXiv:1605.07277v1*, 2016. 1

[56] N. Papernot, P. McDaniel, I. Goodfellow, S. Jha, Z. B. Celik, and A. Swami. Practical black-box attacks against machine learning. In *Proceedings of the 2017 ACM on Asia Conference on Computer and Communications Security*. ACM, 2017. 2, 3, 8

[57] N. Papernot, P. McDaniel, X. Wu, S. Jha, and A. Swami. Distillation as a defense to adversarial perturbations against deep neural networks. In *IEEE Symposium on Security and Privacy*, 2016. 1, 2, 8

[58] A. Paszke, A. Chaurasia, S. Kim, and E. Culurciello. Enet: A deep neural network architecture for real-time semantic segmentation. In *arXiv preprint arXiv:1606.02147v1*, 2016. 4, 6, 12

[59] M. Sharif, S. Bhagavatula, L. Bauer, and M. K. Reiter. Accessorize to a crime: Real and stealthy attacks on state-of-the-art face recognition. In *Proceedings of the 23rd ACM SIGSAC Conference on Computer and Communications Security*, 2016. 1

[60] E. Shelhamer, J. Long, and T. Darrell. Fully convolutional networks for semantic segmentation. *PAMI*, 39(4):640–651, 2017. 11

[61] E. Shelhamer, K. Rakelly, J. Hoffman, and T. Darrell. Clockwork convnets for video semantic segmentation. In *ECCV 2016 Workshop*, pages 852–868. Springer, 2016. 11, 12

[62] K. Simonyan and A. Zisserman. Very deep convolutional networks for large-scale image recognition. In *ICLR*, 2015. 1, 4

[63] C. Szegedy, W. Zaremba, I. Sutskever, J. Bruna, D. Erhan, I. Goodfellow, and R. Fergus. Intriguing properties of neural networks. In *ICLR*, 2014. 1, 2, 3, 5

[64] F. Tramèr, A. Kurakin, N. Papernot, D. Boneh, and P. McDaniel. Ensemble adversarial training: Attacks and defenses. In *arXiv preprint arXiv:1705.07204v2*, 2017. 3, 5

[65] C. Xie, J. Wang, Z. Zhang, Z. Ren, and A. Yuille. Mitigating adversarial effects through randomization. In *ICLR*, 2018. 7

[66] C. Xie, J. Wang, Z. Zhang, Y. Zhou, L. Xie, and A. Yuille. Adversarial examples for semantic segmentation and object detection. In *ICCV*, 2017. 3

[67] W. Xu, D. Evans, and Y. Qi. Feature squeezing: Detecting adversarial examples in deep neural networks. In *arXiv preprint arXiv:1704.01155v1*, 2017. 3

[68] X. Xu, X. Chen, C. Liu, A. Rohrbach, T. Darell, and D. Song. Can you fool ai with adversarial examples on a visual turing test? In *arXiv preprint arXiv:1709.08693v1*, 2017. 3

[69] F. Yu and V. Koltun. Multi-scale context aggregation by dilated convolutions. In *ICLR*, 2016. 1, 2, 4, 6, 11, 12, 13, 16, 17

[70] H. Zhao, X. Qi, X. Shen, J. Shi, and J. Jia. Icnet for real-time semantic segmentation on high-resolution images. In *arXiv preprint arXiv:1704.08545v1*, 2017. 2, 4, 6, 12, 16

[71] H. Zhao, J. Shi, X. Qi, X. Wang, and J. Jia. Pyramid scene parsing network. In *CVPR*, 2017. 1, 2, 4, 5, 6, 11, 12, 13, 16

[72] S. Zheng, S. Jayasumana, B. Romera-Paredes, V. Vineet, Z. Su, D. Du, C. Huang, and P. Torr. Conditional random fields as recurrent neural networks. In *ICCV*, 2015. 1, 2, 3, 4, 7, 8, 11, 12, 25

Appendix

This supplementary material details the DNN models we analysed, and experiments we omitted from the main paper since they follow similar trends. Section A provides further details about the experimental set-up, including the various DNNs used in the experiments. Section B shows qualitative examples of the adversarial attacks we studied. Section C presents further experimental results about "The robustness of different networks" (Sec. 5 of the main paper). Similarly, Section D shows more experimental results about "Multi-scale Processing and Transferability of Adversarial Examples" (Sec. 6 of the main paper). Finally, Section E presents further experimental results on the "Effect of CRFs on Adversarial Robustness" (Sec. 7 of the main paper).

A. Experimental setup

This section details the DNN models, additional information about the Cityscapes dataset and the software and hardware used in the experiments.

A.1. Software and hardware setup

We use the Caffe [38] deep learning framework for all experiments, since most publicly available segmentation models are implemented using this library. Our experiments are performed on either a Nvidia M40 or P100 GPU which have 12GB and 16GB of memory respectively.

A.2. Description of models

We detail each model in this section. Tab. 2 shows the performance of publicly available models on the Pascal VOC validation set. Tab. 3 compares the Intersection over Union (IoU) obtained by models that we have retrained compared to the original author's performance where available. Tab. 4 shows the performance of publicly available models on the Cityscapes validation set. Finally, Tab. 5 lists the number of parameters in each of the models.

FCN8s [47]. We retrained the FCN8s (VGG) network on Pascal VOC with additional annotations from SBD [32] and MS-COCO [45]. The publicly available model of FCN8s is not trained with MS-COCO, which is why we retrained it ourselves. As shown in Tab. 3, we obtain an IoU of 68.7% on the VOC validation set, whilst the original authors who did not train on MS-COCO obtained 65.5% [60].

For the Cityscapes dataset, we used the publicly available VGG model[2] from [61].

We trained FCN8s with a ResNet-101 backbone on Pascal VOC since no publicly available model was available. As shown in Tab. 3, the IoU on clean inputs of this version is close to the VGG version. We are not aware of any other published work to compare this number to.

Table 2: Networks with public models, evaluated on the VOC validation set

Model Name	IoU [%]
CRF-RNN [72]	72.8
Dilated Frontend [69]	67.1
Dilated Context [69]	70.4
SegNet [4]	43.0

Deeplab v2 [15]. We cannot use the publicly released models for the Pascal VOC dataset, since they have been trained on the entire validation set as well. Hence, we use the authors' publicly released training code[3] to retrain their networks without the VOC validation set.

We retrained the Deeplab v2 network with ResNet-101 and VGG backbones on Pascal VOC, achieving similar performance to the original authors as shown in Tab. 3. Note that the authors [15] reported results from ablation experiments on the VOC validation set, which we compare to in Tab. 3. However, these models have never been released.

For CRF post-processing, we used the hyperparameters used by the original authors. As the weights of our trained model are different to the authors, it is possible that different CRF hyperparameters that obtain a higher IoU on the validation set exist.

PSPNet [71]. We used the publicly available model[4] for our experiments on Cityscapes. As the public VOC model has been trained on the entire validation set, we cannot use it for our experiments. Consequently, we retrained this model ourselves achieving comparable results to the original authors (Tab. 3). We followed the training procedure described in the original paper where possible. However, the original authors trained the model using 16 GPUs allowing an effective batch size of 16. Due to our limited computational resources, we could only train on a single GPU using a batch size of 1. The large batch size enabled the original authors to compute better batch statistics for batch normalisation. When using a batch size of 1, the variance in the batch statistics is too high to perform batch normalisation. As a result, we "froze" our batch normalisation layers, and used the batch statistics (mean and variance) of the ImageNet-pretrained ResNet-101 model. This is common practice in training semantic segmentation [15] and ob-

[2] https://github.com/shelhamer/clockwork-fcn
MD5 checksum of Caffe model: fcae4fdc759f9f461fffc7cc3baa96c6

[3] https://bitbucket.org/aquariusjay/deeplab-public-ver2.git

[4] https://github.com/hszhao/PSPNet
MD5 checksum of Caffe model: 29bbdf0ce4d2a6546ed473656db1d6e2

Table 3: Retrained models on VOC validation set. Details about FCN8, Deeplab v2 and PSPNet can be found in Sec. A.2.

Model Name	IoU [%]	IoU of authors [%]
FCN8s (VGG) [47]	68.7	–
FCN8s (ResNet) [47]	68.8	–
Deeplab v2 ASPP (VGG) [15]	66.9	68.9
Deeplab v2 ASPP (ResNet) [15]	73.3	–
Deeplab v2 Multiscale ASPP (ResNet) [15]	73.9	76.3
Deeplab v2 Multiscale ASPP (ResNet) + CRF post-processing [15]	74.9	77.7
PSPNet [71]	75.9	–
PSPNet [71] (test set)	79.0	85.4

Table 4: Networks with public models on Cityscapes validation set. We have reported the IoU at 1024×512 inputs, as well as the original 2048×1024 if the network was trained using full-resolution crops.

Model name	IoU at 1024×512	IoU at 2048×1024
E-Net [58]	53.4	–
ICNet [70]	56.5	67.2
FCN8s (VGG) [61]	62.1	66.4
Dilated Frontend [69]	59.0	64.6
Dilated Context [69]	62.3	68.6
PSPNet [71]	74.4	79.7

ject detection [36] networks where batch sizes are typically small.

As shown in Tab. 3, our reimplementation of PSPNet on VOC achieves comparable results to the original authors, even though it has been trained on 1449 fewer images (the VOC validation set). We compared our implementation to the authors on the held-out test set (evaluation is performed on an online server) as the performance on the validation set is not reported in the original paper.

CRF-RNN [72]. We used the publicly available model for Pascal VOC (trained on MS-COCO)[5].

DilatedNet [69]. We used the public Pascal VOC and Cityscapes models[6].

ICNet [70]. We used the public Cityscapes model[7].

[5] https://github.com/torrvision/crfasrnn
MD5 checksum of Caffe model: bc4926ad00ecc9a1c627db82377ecf56

[6] https://github.com/fyu/dilation.
MD5 checksum for Pascal VOC: 7a44221dbc2611529bff32029ad1f6e2
MD5 checksum for Cityscapes: 0de4d78b5f9692f2aba5e7ed88f93ccb

[7] https://github.com/hszhao/ICNet
MD5 checksum of Caffe model: c7038630c4b6c869afaaadd811bdb539

Table 5: The number of parameters in each of the DNN models evaluated in this paper. As all the networks are stored as 32-bit/4-byte floating point numbers, we reported the number of parameters in megabytes (MB).

Model Name	Dataset	Number of parameters (MB)
E-Net	Cityscapes	1.5
ICNet	Cityscapes	30.1
PSPNet (ResNet-101)	Cityscapes	260.2
Dilated Frontend (VGG)	Cityscapes	512.4
FCN8s (VGG)	Cityscapes	512.5
Dilated Context (VGG)	Cityscapes	512.6
Segnet (VGG)	Pascal	112.4
Deeplab v2 (VGG)	Pascal	144.5
FCN8s (ResNet-101)	Pascal	162.9
Deeplab v2 (ResNet-101)	Pascal	168.4
PSPNet (ResNet-101)	Pascal	272.7
Dilated Frontend (VGG)	Pascal	512.4
FCN8s (VGG)	Pascal	513.0
CRF-RNN (VGG)	Pascal	513.0
Dilated Context (VGG)	Pascal	538.4

E-Net [58]. We used the public Cityscapes model[8].

SegNet [4]. We used the public Pascal VOC model[9].

A.3. Cityscapes dataset

Tab. 4 shows the performance of various publicly available models on the Cityscapes validation set consisting of 500 images. Cityscapes images are captured at a high resolution of 2048×1024, which is too large to fit into GPU memory for most networks. With the exception of E-Net [58] (which is trained on half-resolution images), the other

[8] https://github.com/TimoSaemann/ENet
MD5 checksum of Caffe model: d9aabd630cf6bc29c48ea55a86124e14

[9] https://github.com/alexgkendall/SegNet-Tutorial/blob/master/Example_Models/segnet_model_zoo.md
MD5 checksum of Caffemodel: 6e01077e3cda996f95b2a82ea4641a4c

networks we evaluated are trained on smaller crops of full-resolution images. Thereafter, at test time, authors use different tiling strategies [69, 71] to process parts of an image at full resolution before combining the partial results. To make a fairer comparison between models, we process all images at half-resolution so that tiling is not required. In Tab. 4, we show the IoU at the resolution we tested on, 1024×512. And if the model was also trained on full resolution crops, we also include the IoU of the network on full resolution inputs.

B. Qualitative results

Figure 5 visualises adversarial perturbations of varying ℓ_∞ norms, showing how the perturbations only become visible to the naked eye when the l_∞ of the perturbation, ϵ, is 8 (when viewed on screen). Figure 6 shows the results of the four adversarial attacks considered in this paper when applied on the same image from the Pascal VOC dataset on the Deeplab v2 network. Finally, Fig. 7 compares the outputs of different networks to the Iterative FGSM ll attack for varying values of ϵ on the Cityscapes dataset.

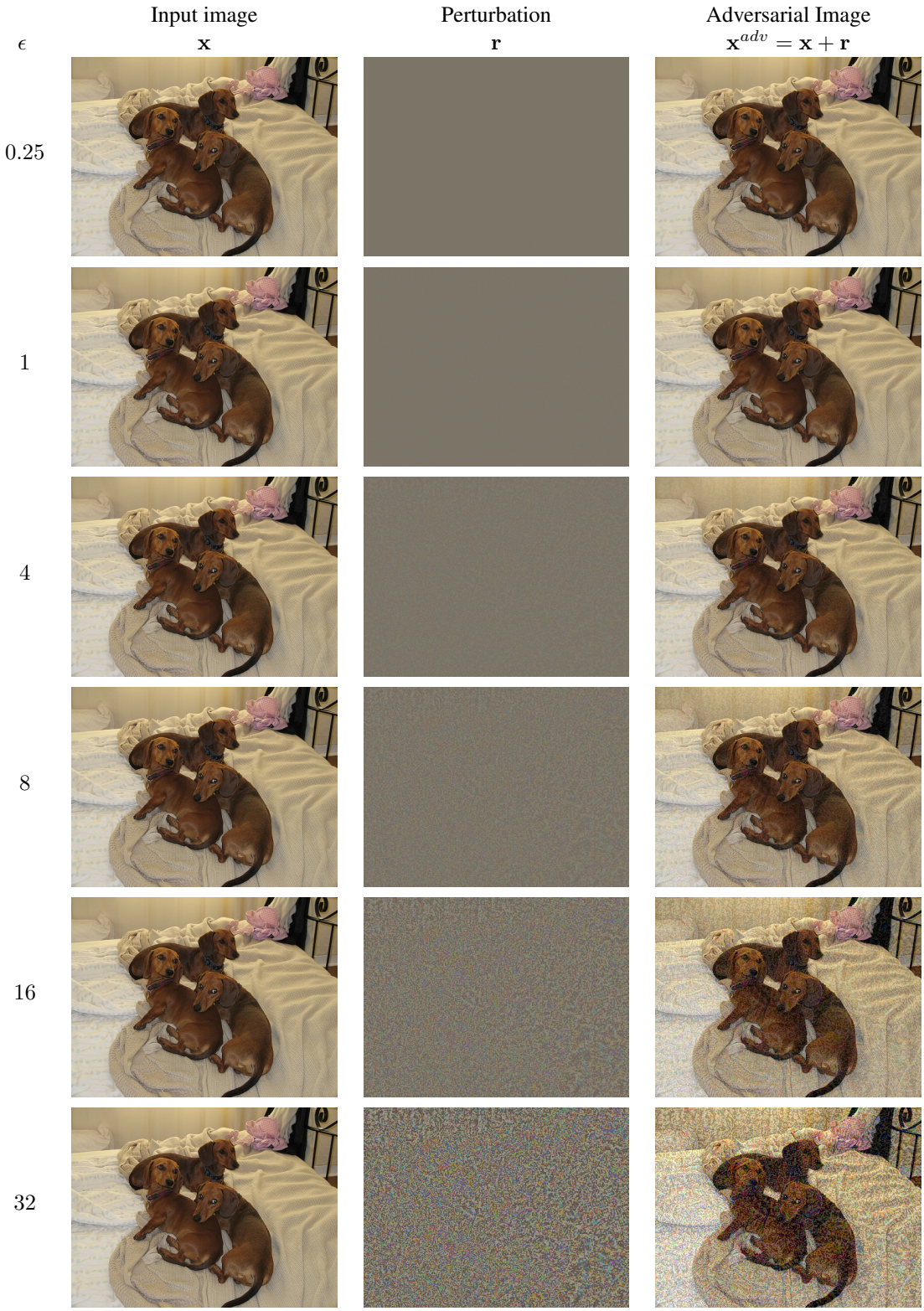

Figure 5: A visualisation of adversarial perturbations of varying ℓ_∞ norms. The perturbation, in the middle column, when added to the input, produces the adversarial example that fools neural networks. Note that the mean RGB value (of the Pascal VOC dataset) is already added to the perturbation, resulting in the grey background. This is required for visualisation as the perturbation can be negative, and RGB images are stored as positive integers $\in [0, 255]$. For $\epsilon = 0.25$, the adversarial image and input image are actually identical if rounded to integers (as RGB images are typically represented). Nevertheless, perturbations of this norm have fooled every neural network studied in this paper. Perturbations become noticeable when viewed on screen at around $\epsilon = 8$. In this figure, perturbations were created using FGSM on Deeplab v2.

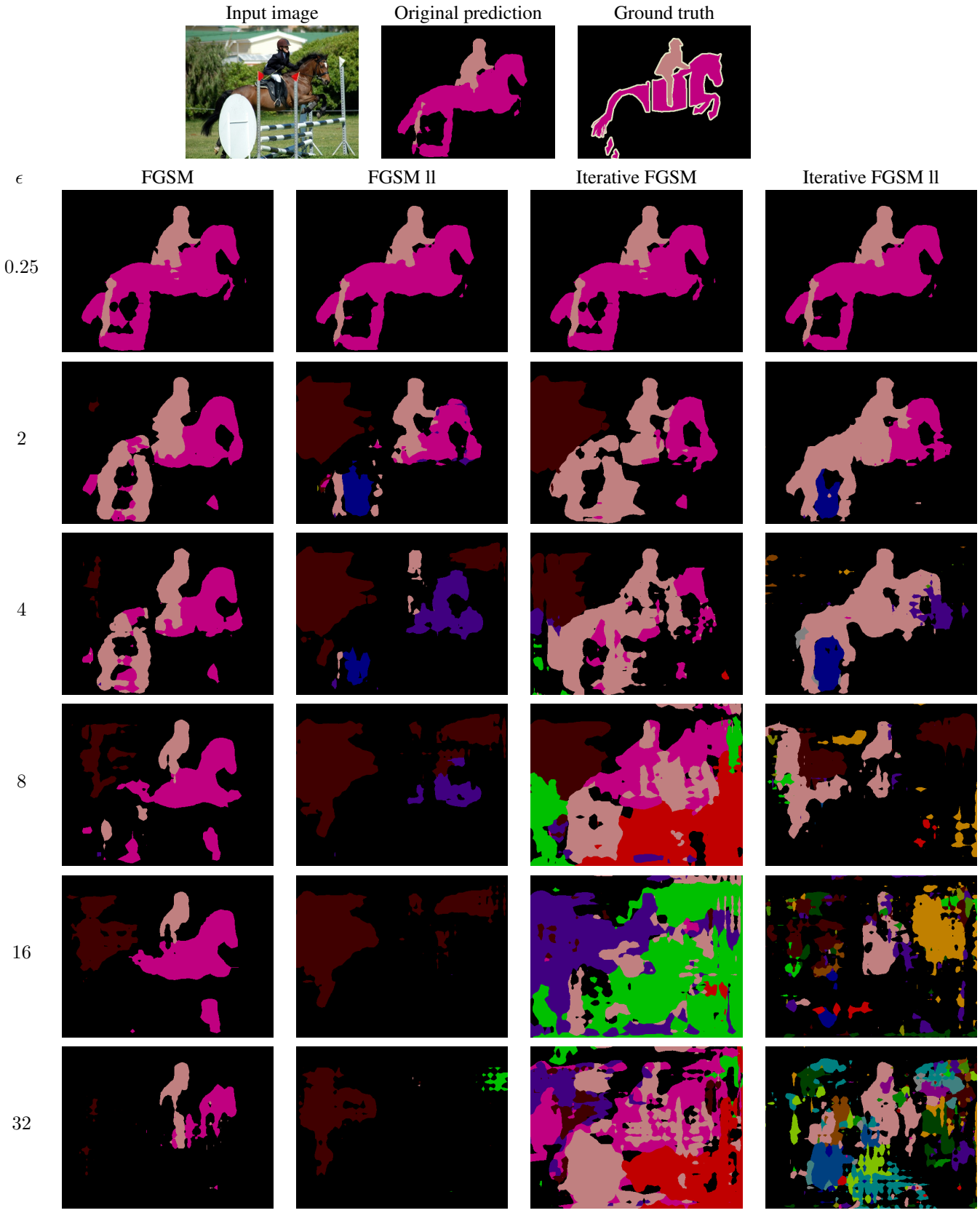

Figure 6: A comparison of different adversarial attacks on the Deeplab v2 Mulitscale ASPP network [15], on a common image from Pascal VOC. As expected, iterative attacks (last two columns) are more effective than single-step ones (first two columns). Higher l_∞ norms of the perturbation, ϵ, also degrade the network's prediction more.

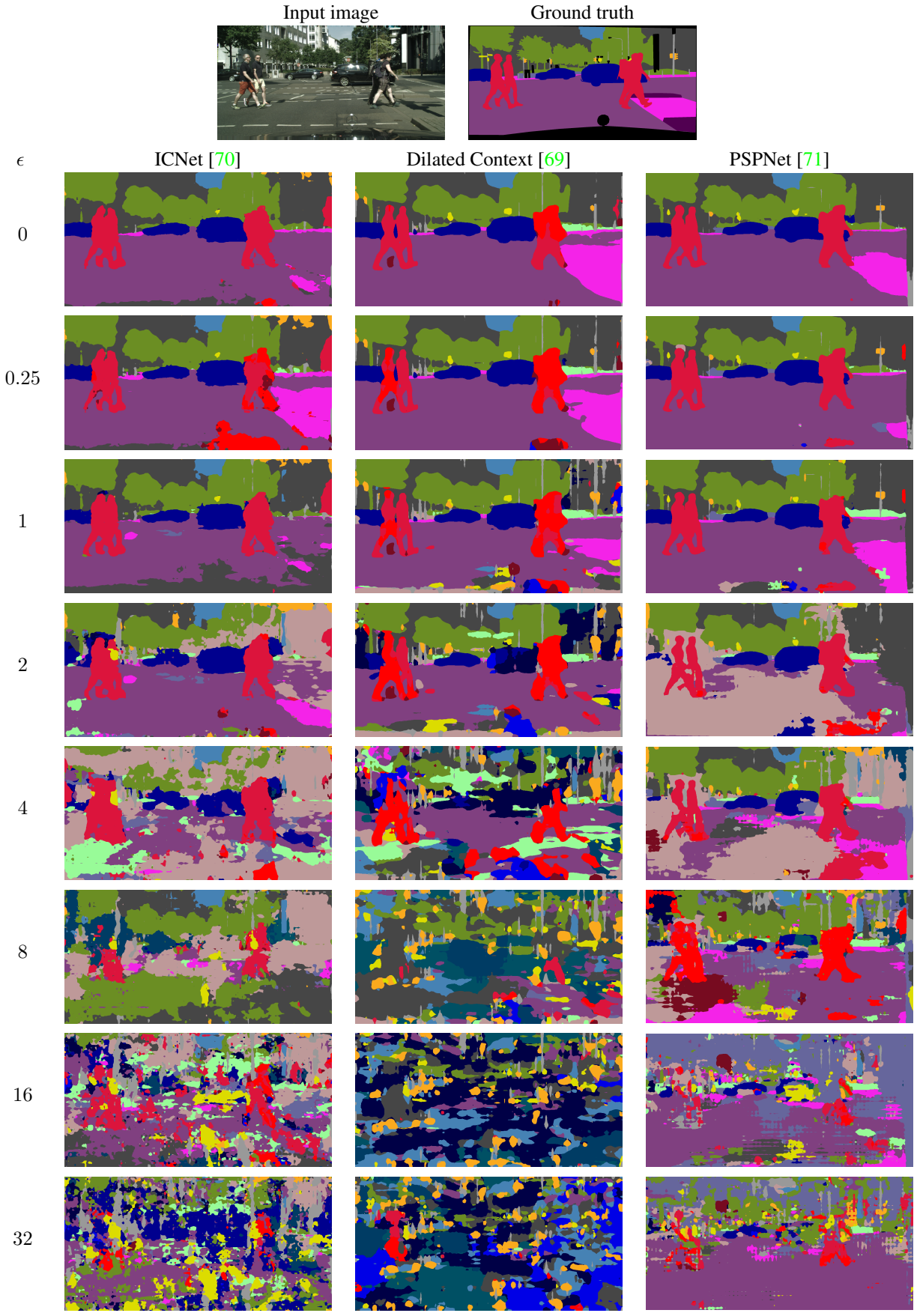

Figure 7: Comparison of ICNet, Dilated Context and PSPNet when attacked by Iterative FGSM ll, for different values of the l_∞ norm, ϵ. Note how each network is affected differently, with PSPNet the most robust. $\epsilon = 0$ is the original prediction of the network, since no perturbation is added here.

C. Robustness of Different Architectures

The main paper presented results using the FGSM and Iterative FGSM ll attacks for both Pascal VOC and Cityscapes datasets. In this section, we present results for the targeted, single-step FGSM ll and untargeted Iterative FGSM attacks as well. Furthermore, we also include the Absolute IoU scores for each attack for different l_∞ perturbations.

C.1. Results of other attacks

Figures 8 and 9 show results of the FGSM ll and Iterative FGSM attacks on the VOC and Cityscapes datasets respectively. Our primary observations from the main paper are mostly consistent on these attacks as well:

- ResNet based networks are more robust than models based on VGG.
- DilatedNet [69] without its "Context" module is typically more robust than the full, more accurate network.
- E-Net and ICNet show similar robustness to DilatedNet on the Cityscapes dataset. It is only for the FGSM ll attack for $\epsilon \geq 4$ that DilatedNet is robust than both of these lightweight networks.
- Single-step attacks (FGSM ll) are particularly effective on Cityscapes at high ϵ values. They are more effective at fooling networks than iterative methods as well. This was unexpected, and not observed on Pascal VOC.
- PSPNet, which achieves the highest IoU on clean inputs, is typically not the most robust network on Pascal VOC.

C.2. Result tables of Absolute IoU

In contrast to the main paper that showed the IoU Ratio for various attacks, Tables 6 through 9 show the absolute IoU for different models for each of the FGSM, FGSM ll, Iterative FGSM and Iterative FGSM ll attacks on the Pascal VOC dataset. Additionally, Tables 10 through 13 show the absolute IoU for different models on the Cityscapes dataset.

Note that PSPNet, which achieves the highest IoU on clean inputs, does not usually achieve the highest absolute IoU when attacked on the Pascal VOC dataset. When considering 4 adversarial attacks, and 8 ϵ values, PSPNet achieves the highest absolute IoU in only 2 out of 32 cases. Moreover, it never achieves the highest absolute IoU for imperceptible perturbations ($0 < \epsilon \leq 4$).

Additionally, the highest absolute IoU for any ϵ value is always from a ResNet-based model (Deeplab v2, FCN8s (ResNet) or PSPNet) on the Pascal VOC dataset. On Cityscapes, FCN8s (VGG) is sometimes the most robust network at high ϵ values. However, the performance of all the networks is severely degraded at this point.

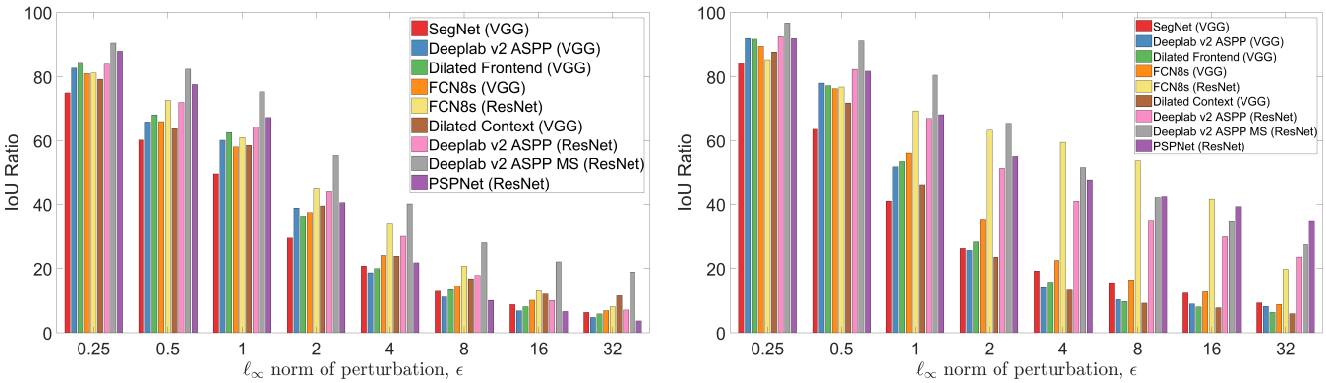

(a) Untargeted Iterative FGSM attack

(b) Targeted FGSM ll. attack

Figure 8: Adversarial robustness of state-of-the-art models on the Pascal VOC dataset. As with the FGSM and Iterative FGSM ll attacks in the main paper, models based on the ResNet backbone are more robust. Deeplab v2 is generally the most robust network, except on the Targeted FGSM attack for $\epsilon \geq 4$. The Iterative FGSM attack is also more effective at fooling the networks than the single-step Targeted FGSM attack, as shown by the lower IoU ratios.

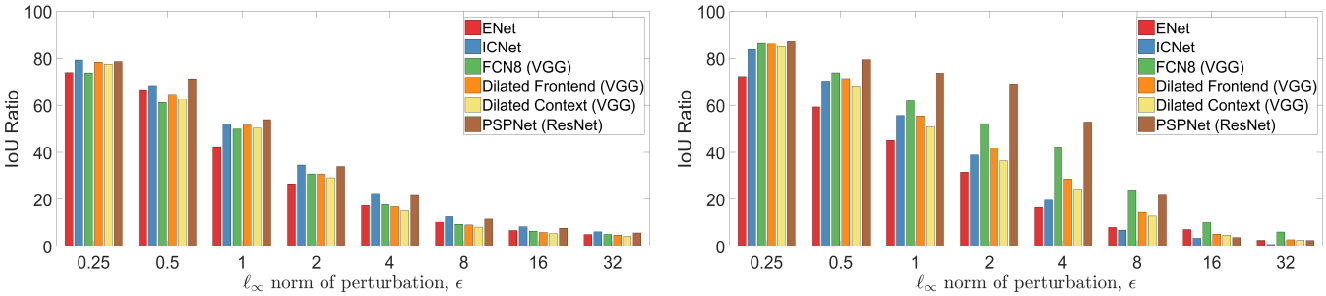

(a) Untargeted Iterative FGSM attack

(b) Targeted FGSM ll. attack

Figure 9: Adversarial robustness of state-of-the-art models on the Cityscapes dataset. As with the FGSM and Iterative FGSM ll attacks in the main paper, PSPNet is typically the most robust. Once again, DilatedNet without its "Context" module is slightly more robust than the full, more accurate network. The single-step FGSM ll attack is also more effective at higher ϵ values than the Iterative FGSM attack. This is unexpected, but was also observed in the main paper between the FGSM and Iterative FGSM ll attacks.

Table 6: The absolute IoU on the *Pascal VOC* dataset for various models when attacked with *FGSM*. This is evaluated for eight different values of the ℓ_∞ norm of the perturbation, ϵ. $\epsilon = 0$ represents the IoU on clean inputs.

Network	ℓ_∞ norm of perturbation, ϵ								
	0	0.25	0.5	1	2	4	8	16	32
SegNet (VGG)	43.0	32.3	25.9	19.5	14.8	11.7	9.7	6.9	4.0
Deeplab v2 ASPP (VGG)	66.9	55.3	44.1	31.7	22.5	17.2	13.9	11.8	9.1
Dilated Frontend (VGG)	67.1	56.7	45.7	33.8	24.2	19.2	16.1	12.2	8.2
FCN8s (VGG)	68.7	55.7	45.4	36.1	28.8	23.9	19.9	16.1	10.3
FCN8s (ResNet)	68.8	55.9	49.9	44.2	39.5	35.9	32.0	24.8	12.8
Dilated Context (VGG)	70.4	55.8	44.9	34.4	26.0	20.6	17.2	13.9	9.0
Deeplab v2 ASPP (ResNet)	73.3	61.6	52.7	43.3	35.9	30.7	27.7	24.6	18.5
Deeplab v2 ASPP MS (ResNet)	73.9	**66.9**	**60.9**	**54.1**	**47.9**	**43.2**	**39.2**	**35.7**	**28.5**
PSPNet (ResNet)	**75.9**	66.8	59.0	48.9	39.8	33.8	29.2	26.7	21.2

Table 7: The absolute IoU on the *Pascal VOC* dataset for various models when attacked with *FGSM ll*. This is evaluated for eight different values of the ℓ_∞ norm of the perturbation, ϵ. $\epsilon = 0$ represents the IoU on clean inputs.

Network	ℓ_∞ norm of perturbation, ϵ								
	0	0.25	0.5	1	2	4	8	16	32
SegNet (VGG)	43.0	36.2	27.4	17.6	11.4	8.3	6.7	5.4	4.1
Deeplab v2 ASPP (VGG)	66.9	61.5	52.3	34.6	17.3	9.5	7.0	6.1	5.6
Dilated Frontend (VGG)	67.1	61.6	51.9	35.8	19.1	10.6	6.6	5.5	4.4
FCN8s (VGG)	68.7	61.5	52.5	38.6	24.4	15.5	11.4	8.8	6.2
FCN8s (ResNet)	68.8	58.7	52.9	47.7	43.6	**41.0**	**36.8**	28.6	13.6
Dilated Context (VGG)	70.4	61.7	50.5	32.5	16.5	9.4	6.6	5.6	4.3
Deeplab v2 ASPP (ResNet)	73.3	67.8	60.4	49.1	37.5	30.0	25.7	22.0	17.2
Deeplab v2 ASPP MS (ResNet)	73.9	**71.5**	**67.4**	**59.5**	**48.4**	38.0	31.1	25.8	20.4
PSPNet (ResNet)	**75.9**	69.8	62.1	51.8	41.8	36.2	32.1	**29.8**	**26.6**

Table 8: The absolute IoU on the *Pascal VOC* dataset for various models when attacked with *Iterative FGSM*. This is evaluated for eight different values of the ℓ_∞ norm of the perturbation, ϵ. $\epsilon = 0$ represents the IoU on clean inputs.

Network	ℓ_∞ norm of perturbation, ϵ								
	0	0.25	0.5	1	2	4	8	16	32
SegNet (VGG)	43.0	32.3	25.9	21.3	12.7	8.9	5.6	3.8	2.8
Deeplab v2 ASPP (VGG)	66.9	55.3	44.1	40.3	26.0	12.5	7.6	4.7	3.4
Dilated Frontend (VGG)	67.1	56.7	45.7	42.1	24.4	13.4	9.1	5.6	4.1
FCN8s (VGG)	68.7	55.7	45.4	39.9	25.8	16.5	10.0	7.1	4.9
FCN8s (ResNet)	68.8	55.9	49.9	42.0	31.0	23.3	14.2	9.1	5.7
Dilated Context (VGG)	70.4	55.8	44.9	41.2	27.8	16.7	11.9	8.6	8.2
Deeplab v2 ASPP (ResNet)	73.3	61.6	52.7	47.3	32.2	22.1	13.1	7.5	5.3
Deeplab v2 ASPP MS (ResNet)	73.9	**66.9**	**60.9**	**55.8**	**40.9**	**29.6**	**20.9**	**16.3**	**14.0**
PSPNet (ResNet)	**75.9**	66.8	59.0	51.1	30.8	16.5	7.8	5.2	2.8

Table 9: The absolute IoU on the *Pascal VOC* dataset for various models when attacked with *Iterative FGSM ll*. This is evaluated for eight different values of the ℓ_∞ norm of the perturbation, ϵ. $\epsilon = 0$ represents the IoU on clean inputs.

Network	ℓ_∞ norm of perturbation, ϵ								
	0	0.25	0.5	1	2	4	8	16	32
SegNet (VGG)	43.0	36.2	27.4	22.0	11.4	6.7	5.3	4.1	3.7
Deeplab v2 ASPP (VGG)	66.9	61.5	52.3	49.0	28.0	12.1	6.7	5.8	4.8
Dilated Frontend (VGG)	67.1	61.6	51.9	49.1	27.8	10.8	5.4	4.0	3.7
FCN8s (VGG)	68.7	61.5	52.5	52.5	33.0	17.1	10.4	8.4	6.8
FCN8s (ResNet)	68.8	58.7	52.9	47.8	37.6	28.9	**18.2**	**12.2**	**7.9**
Dilated Context (VGG)	70.4	61.7	50.5	48.9	22.9	9.2	5.6	5.0	4.1
Deeplab v2 ASPP (ResNet)	73.3	67.8	60.4	56.9	39.6	21.1	11.3	7.7	6.3
Deeplab v2 ASPP MS (ResNet)	73.9	**71.5**	**67.4**	**65.2**	**52.6**	**30.2**	15.5	9.1	7.1
PSPNet (ResNet)	**75.9**	69.8	62.1	58.5	37.2	20.0	11.1	7.9	5.1

Table 10: The absolute IoU on the *Cityscapes* dataset for various models when attacked with *FGSM*. This is evaluated for eight different values of the ℓ_∞ norm of the perturbation, ϵ. $\epsilon = 0$ represents the IoU on clean inputs.

Network	ℓ_∞ norm of perturbation, ϵ								
	0	0.25	0.5	1	2	4	8	16	32
ENet	53.4	39.6	35.6	31.0	24.0	13.2	5.8	4.1	1.4
ICNet	56.5	47.0	41.3	35.5	28.5	16.8	4.5	2.4	0.8
FCN8 (VGG)	62.1	46.0	38.0	31.9	27.8	23.9	**16.2**	**7.7**	**3.9**
Dilated Frontend (VGG)	59.0	46.3	38.1	31.1	25.7	20.7	13.3	5.0	1.7
Dilated Context (VGG)	62.3	48.4	39.0	31.6	26.0	20.8	13.3	4.8	1.8
PSPNet (ResNet)	**74.4**	**58.5**	**52.9**	**48.9**	**46.0**	**36.3**	16.0	2.8	1.9

Table 11: The absolute IoU on the *Cityscapes* dataset for various models when attacked with *FGSM ll*. This is evaluated for eight different values of the ℓ_∞ norm of the perturbation, ϵ. $\epsilon = 0$ represents the IoU on clean inputs.

Network	ℓ_∞ norm of perturbation, ϵ								
	0	0.25	0.5	1	2	4	8	16	32
ENet	53.4	38.5	31.7	24.2	17.0	8.9	4.3	3.8	1.4
ICNet	56.5	47.2	40.5	33.2	25.1	13.4	3.4	2.3	0.8
FCN8 (VGG)	62.1	53.8	46.0	38.4	32.5	26.3	14.9	**6.4**	**3.8**
Dilated Frontend (VGG)	59.0	50.9	42.0	32.8	24.6	16.8	8.7	3.1	1.7
Dilated Context (VGG)	62.3	53.2	42.5	31.8	22.8	15.1	8.2	3.0	1.7
PSPNet (ResNet)	**74.4**	**64.9**	**59.1**	**55.0**	**51.3**	**39.5**	**16.5**	2.8	1.9

Table 12: The absolute IoU on the *Cityscapes* dataset for various models when attacked with *Iterative FGSM*. This is evaluated for eight different values of the ℓ_∞ norm of the perturbation, ϵ. $\epsilon = 0$ represents the IoU on clean inputs.

Network	ℓ_∞ norm of perturbation, ϵ								
	0	0.25	0.5	1	2	4	8	16	32
ENet	53.4	39.6	35.6	22.6	14.2	9.3	5.7	3.6	2.7
ICNet	56.5	47.0	41.3	30.9	22.4	13.6	7.6	4.8	3.4
FCN8 (VGG)	62.1	46.0	38.0	31.1	19.1	11.1	5.8	4.0	3.2
Dilated Frontend (VGG)	59.0	46.3	38.1	30.6	18.1	10.0	5.4	3.5	2.8
Dilated Context (VGG)	62.3	48.4	39.0	31.4	18.1	9.6	5.1	3.4	2.7
PSPNet (ResNet)	**74.4**	**58.5**	**52.9**	**40.2**	**25.4**	**16.4**	**8.9**	**5.7**	**4.3**

Table 13: The absolute IoU on the *Cityscapes* dataset for various models when attacked with *Iterative FGSM ll*. This is evaluated for eight different values of the ℓ_∞ norm of the perturbation, ϵ. $\epsilon = 0$ represents the IoU on clean inputs.

Network	ℓ_∞ norm of perturbation, ϵ								
	0	0.25	0.5	1	2	4	8	16	32
ENet	53.4	38.5	31.7	19.2	14.6	9.2	5.1	3.5	2.7
ICNet	56.5	47.2	40.5	33.8	22.4	14.5	8.9	6.8	5.5
FCN8 (VGG)	62.1	53.8	46.0	36.5	24.8	14.0	7.7	5.9	4.9
Dilated Frontend (VGG)	59.0	50.9	42.0	31.8	20.0	10.5	5.3	4.7	4.0
Dilated Context (VGG)	62.3	53.2	42.5	32.2	19.9	8.8	4.8	3.6	2.8
PSPNet (ResNet)	**74.4**	**64.9**	**59.1**	**46.1**	**36.5**	**26.1**	**16.9**	**11.5**	**8.8**

D. Multiscale Processing and Transferability of Adversarial Examples

This section details additional results with both Deeplab v2 and FCN8s.

D.1. Deeplab v2

Table 14 shows the performance, measured in IoU, on the VOC validation set when the input image is processed at different resolutions (50%, 75%, 100%). The fact that a different IoU is obtained for each input resolution, even though the weights of the network are the same, confirms that the network is not scale invariant. Note that the version of Deeplab which processes images at all the aforementioned resolutions, and max-pools the prediction at each pixel obtains the highest IoU. An alternative to max-pooling the predictions from each scale is to average-pool them. This method gives an insignificant improvement in accuracy, but does improve robustness as shown in Fig. 10.

Table 14: Performance of Deeplab v2 (ResNet) on the VOC validation set when processing images at different resolutions

Model Name	IoU [%]
Deeplab v2 50% scale	67.8
Deeplab v2 75% scale	71.9
Deeplab v2 100% scale	73.3
Deeplab v2 100% scale (average pooling)	73.4
Deeplab v2 Multiscale (max pooling)	73.9

D.1.1 Average-pooling instead of max-pooling

As shown in Fig. 10, average-pooling the results from each scale is also more robust to all the adversarial attacks we tested compared to the single-scale version of Deeplab v2. In fact, multiscale processing (either max- or average-pooling) achieves a higher IoU Ratio at almost all ϵ values for each attack.

Table 16 also shows that black-box attacks generated from multiscale-averaging also transfer better to single scales of Deeplab v2, for all four adversarial attacks considered in this paper. This is similar to the case of max-pooling as shown in the main paper.

D.1.2 Transferability experiments using the FGSM ll and Iterative FGSM attacks

Table 17 shows the transferability of adversarial attacks to different scales of Deeplab v2 using the FGSM ll and Iterative FGSM attacks. The main paper presented results using the FGSM and Iterative FGSM ll attacks. However, our findings remain consistent on these different attacks. The multiscale version of Deeplab v2 is the most robust to these attacks (as also seen in Fig. 8 and 10), and black-box attacks from it transfer the best to other scales of Deeplab v2.

Table 15: Performance of FCN8s when processing images at different resolutions. As with Deeplab v2, max-pooling the predictions from multiple scales achieves the best results.

Model Name	IoU [%]
FCN8s 50% scale	60.8
FCN8s 75% scale	67.8
FCN8s 100% scale	68.7
FCN8s Multiscale	69.9

D.1.3 Transferability experiments at multiple ϵ values

Figure 11 shows the results of black-box attacks for multiple ϵ values between different scales of Deeplab v2 for the FGSM attack. The results are largely consistent with those at $\epsilon = 8$ as reported in the main paper – the multiscale version of Deeplab v2 is the most robust to white-box attacks and black-box attacks generated from it transfer the best to other scales of Deeplab v2. Also note how the transferability from each scale to another varies greatly. For example, attacks generated from the 50% scale transfer very poorly to 100% and vice versa.

D.2. FCN8s

Table 15 shows the IoU of FCN8s (VGG) as the input resolution of the image is varied from the VOC dataset. As with Deeplab v2, a multiscale version which max-pools the predictions from each scale achieves the highest IoU.

The transferability experiments from Section 6 of the paper are repeated on FCN8 in Tables 18 and 19. Note that FCN8s has not been trained in a multiscale manner as Deeplab v2, and it is rather done as a post-processing step. Nevertheless, the results show a similar trend as Deeplab v2: The multiscale network is more robust to white-box attacks and black-box attacks generated from it transfer better. This suggests that training the network in a multiscale manner does not confer robustness to adversarial examples. Rather it is the fact that CNNs are not scale invariant, and that adversarial examples generated at one scale are not as malignant at another. Finally Fig. 12 shows the transferability experiments at multiple ϵ values, as was done for Deeplab v2 in the previous subsection.

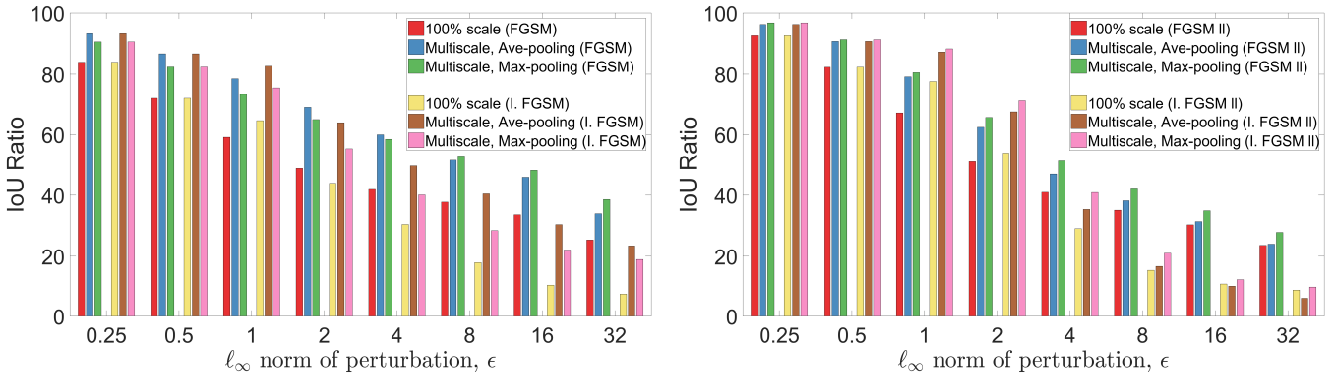

(a) Untargeted attacks

(b) Targeted attacks

Figure 10: Adversarial robustness of Deeplab ASPP (single-scale) and Deeplab Multiscale ASPP. We compare two types of multiscale ensembling – max-pooling and average-pooling the predictions from each of the three scales of Deeplab v2 (ResNet 101). Note that both average- and max-pooling are more robust than just a single-scale model, achieving higher IoU Ratios for almost every ϵ value for each attack on the Pascal VOC dataset.

Table 16: Transferability of adversarial examples generated from different scales of Deeplab v2 (columns) and evaluated on different networks (rows). In this case, the outputs from each scale are *average-pooled* instead of max-pooled. The underlined diagonals for each attack show white-box attacks. Off-diagonals, show transfer (black-box) attacks. The most effective one in bold, is typically from the multiscale version of Deeplab v2. In the case of Iterative FGSM ll, black-box attacks from the multiscale networks are sometimes even more effective than white-box ones.

Network evaluated	FGSM ($\epsilon = 8$)				Iterative FGSM ll ($\epsilon = 8$)			
	50%	75%	100%	Multiscale	50%	75%	100%	Multiscale
Deeplab v2 0.5 (ResNet)	<u>37.3</u>	70.5	84.8	**48.8**	<u>18.0</u>	92.0	96.9	**12.1**
Deeplab v2 0.75 (ResNet)	85.5	<u>39.7</u>	62.2	**54.2**	99.5	<u>17.9</u>	89.9	**17.4**
Deeplab v2 1 (ResNet)	93.6	57.9	<u>37.7</u>	**51.7**	100.0	79.0	<u>15.5</u>	**9.6**
Deeplab v2 Multiscale (ResNet)	75.1	**54.2**	59.0	<u>51.6</u>	95.2	**84.9**	87.5	<u>16.7</u>
Network evaluated	FGSM ll ($\epsilon = 8$)				Iterative FGSM ($\epsilon = 8$)			
	50%	75%	100%	Multiscale	50%	75%	100%	Multiscale
Deeplab v2 50% (ResNet)	<u>36.4</u>	70.1	83.7	**36.6**	<u>21.3</u>	90.9	97.0	**37.3**
Deeplab v2 75% (ResNet)	89.9	<u>37.4</u>	61.6	**39.9**	99.1	<u>20.0</u>	88.6	**44.1**
Deeplab v2 100% (ResNet)	95.1	58.3	<u>35.1</u>	**36.9**	100.2	71.9	<u>18.6</u>	**33.5**
Deeplab v2 Multiscale (ResNet)	96.0	**91.4**	94.7	<u>38.2</u>	94.5	**76.2**	86.5	<u>37.7</u>

Table 17: Transferability of adversarial examples generated from different scales of Deeplab v2 (columns) and evaluated on different networks (rows). As with the main paper, *max-pooling* is performed from the output of each scale. However, in contrast to the main paper, the FGSM ll and Iterative FGSM attacks are reported. The underlined diagonals for each attack show white-box attacks. Off-diagonals, show transfer (black-box) attacks. The most effective one in bold, is typically from the multiscale version of Deeplab v2.

Network evaluated	FGSM ll ($\epsilon = 8$)				Iterative FGSM ($\epsilon = 8$)			
	50%	75%	100%	Multiscale	50%	75%	100%	Multiscale
Deeplab v2 0.5 (ResNet)	<u>36.4</u>	70.1	83.7	**46.0**	<u>21.3</u>	90.9	97.0	**39.2**
Deeplab v2 0.75 (ResNet)	89.9	<u>37.4</u>	61.6	**43.3**	99.1	<u>20.0</u>	88.6	**34.0**
Deeplab v2 1 (ResNet)	95.1	58.3	<u>35.1</u>	**33.9**	100.2	71.9	<u>18.6</u>	**22.0**
Deeplab v2 Multiscale (ResNet)	90.7	**60.8**	68.9	<u>42.1</u>	96.5	**81.9**	87.5	<u>29.2</u>
Deeplab v2 (VGG)	95.1	69.9	63.8	**61.9**	98.5	86.9	86.3	**81.2**
FCN8 (VGG)	94.5	67.7	64.7	**62.4**	98.7	86.9	86.0	**82.0**

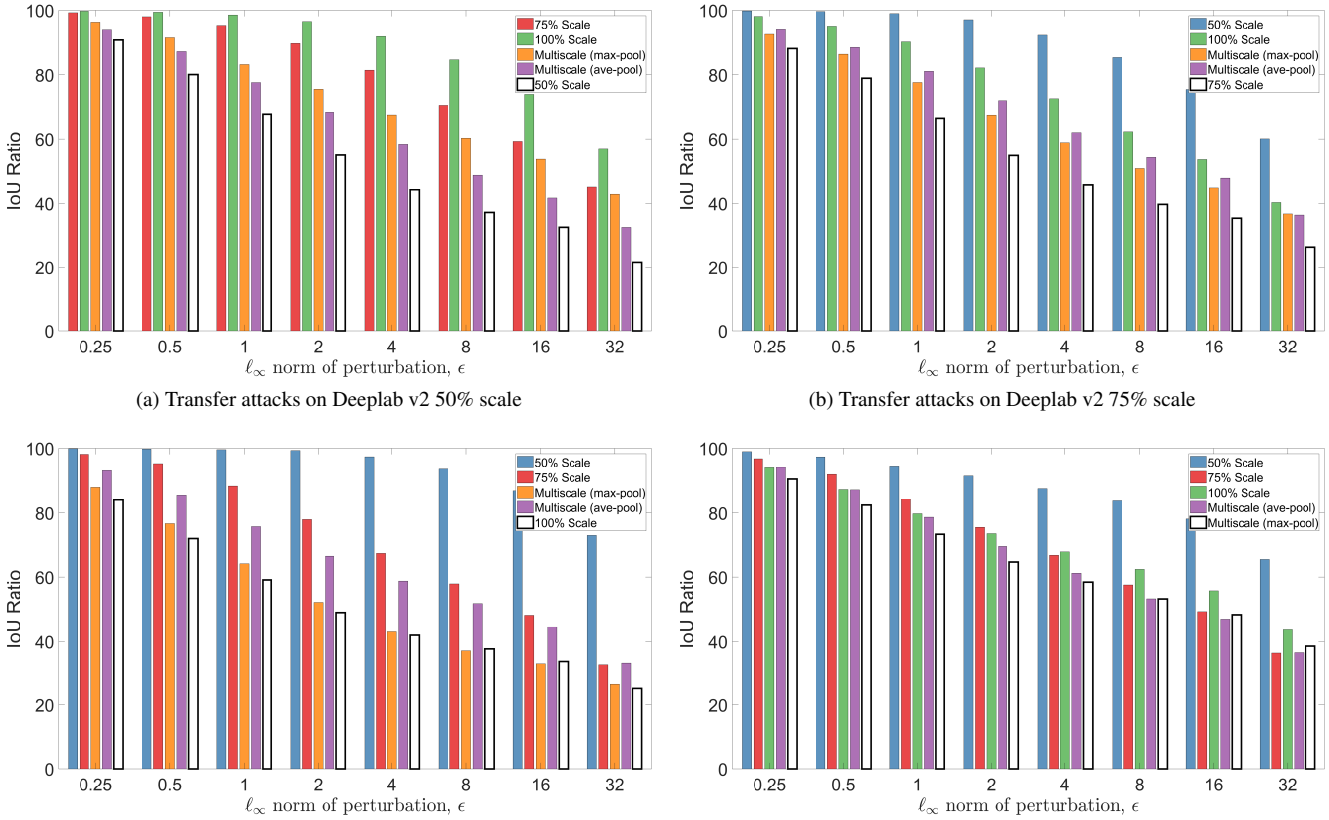

(a) Transfer attacks on Deeplab v2 50% scale

(b) Transfer attacks on Deeplab v2 75% scale

(c) Transfer attacks on Deeplab v2 100% scale

(d) Transfer attacks on Deeplab v2 Multiscale (max-pooling)

Figure 11: Black-box attacks on each scale of Deeplab v2, from each other scale, using adversarial perturbations generated by FGSM for differing values of ϵ on the Pascal VOC dataset. In each figure, the last bar shows the "white-box" attack on the network, where the attack is generated from the network that is being evaluated. This is typically the most powerful attack, as expected. Note that attacks generated from the multiscale version of Deeplab v2 (using either max- or average-pooling) produce the most effective black-box attacks across multiple ϵ values. The trend from the main paper, which only tabulated the IoU Ratio for $\epsilon = 8$, can thus be seen across all other ϵ values considered in this paper.

Table 18: Transferability of adversarial examples generated from different scales of FCN8s (VGG) (columns) and evaluated on different networks (rows) on the Pascal VOC dataset. For the multiscale network, the outputs from each scale are max-pooled. The underlined diagonals for each attack show white-box attacks. Off-diagonals, show transfer (black-box) attacks. The most effective one in bold, is typically from the multiscale version of FCN8s.

Network evaluated	FGSM ($\epsilon = 8$)				Iterative FGSM ll ($\epsilon = 8$)			
	50%	75%	100%	Multiscale	50%	75%	100%	Multiscale
FCN8 50%	<u>32.1</u>	**53.3**	81.0	53.7	<u>20.5</u>	87.3	96.9	**21.9**
FCN8 75%	78.4	<u>30.9</u>	45.5	**40.5**	96.3	<u>17.6</u>	77.8	**20.5**
FCN8 100%	94.0	41.7	<u>28.9</u>	**28.7**	98.2	58.6	<u>15.3</u>	**17.5**
FCN8 Multiscale	79.1	**42.8**	53.3	<u>47.8</u>	97.5	**79.3**	85.2	<u>20.0</u>

Table 19: Transferability of adversarial examples generated from different scales of FCN8s (VGG) (columns) and evaluated on different networks (rows) on the Pascal VOC dataset. For the multiscale network, the outputs from each scale are max-pooled. The underlined diagonals for each attack show white-box attacks. Off-diagonals, show transfer (black-box) attacks. The most effective one in bold, is typically from the multiscale version of FCN8s.

Network evaluated	FGSM ll ($\epsilon = 8$)				Iterative FGSM ($\epsilon = 8$)			
	50%	75%	100%	Multiscale	50%	75%	100%	Multiscale
FCN8 50%	<u>18.5</u>	51.4	79.2	**24.0**	<u>23.6</u>	85.7	97.1	**38.1**
FCN8 75%	80.9	<u>18.5</u>	37.0	**23.4**	97.3	<u>15.9</u>	74.7	**28.1**
FCN8 100%	93.0	33.8	<u>16.6</u>	**17.1**	99.1	54.9	<u>14.7</u>	**18.1**
FCN8 Multiscale	87.5	**40.0**	60.3	<u>21.1</u>	96.4	**74.5**	82.3	<u>25.1</u>

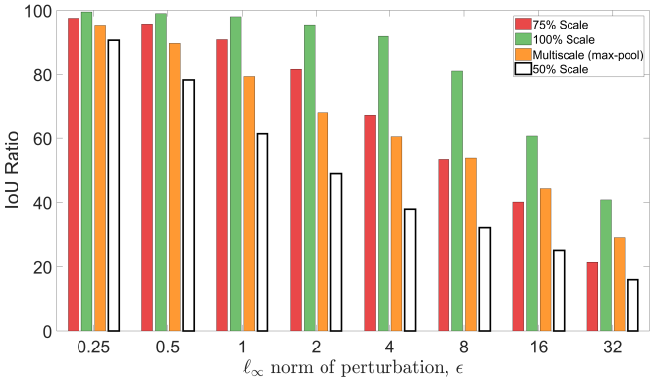

(a) Transfer attacks on FCN8s 50% scale

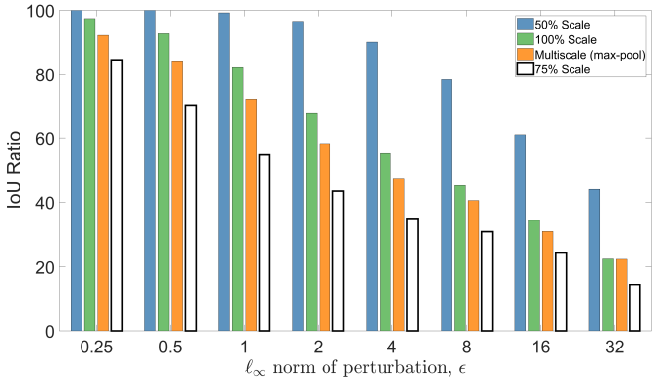

(b) Transfer attacks on FCN8s 75% scale

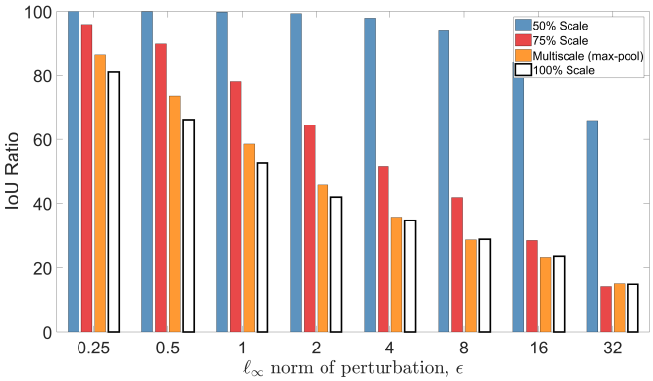

(c) Transfer attacks on FCN8s 100% scale

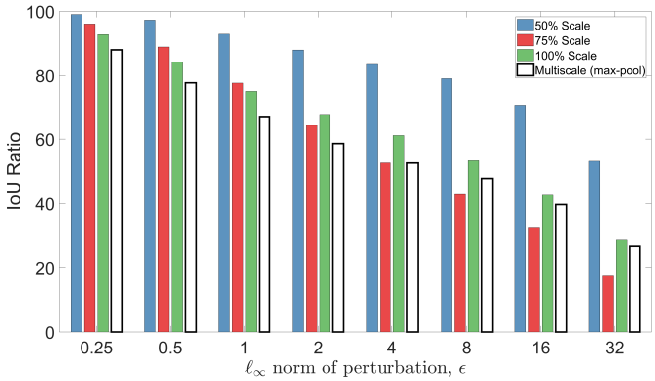

(d) Transfer attacks on FCN8s Multiscale (max-pooling)

Figure 12: Black-box attacks on each scale of FCN8, from each other scale, using adversarial perturbations generated by FGSM for differing values of ϵ on the Pascal VOC dataset. In each figure, the last bar shows the "white-box" attack on the network, where the attack is generated from the network that is being evaluated. The results from this experiment are very similar to Deeplab v2 – attacks generated from the multiscale network transfer the best to other scales. However, unlike Deeplab v2, the FCN8s network in this case was not trained with multiscale ensembling. This was simply done at test-time. This suggests that the increased robustness of multiscale networks to adversarial attacks, and their transferability to other networks, is not a result of the training procedure, but rather the fact that these networks are not scale invariant.

E. Effect of CRFs on Adversarial Robustness

E.1. Adversarial Robustness and Smoothing

The pairwise term of DenseCRF [40] (which is interpreted as a neural network in CRF-RNN [72]) takes the form of a weighted sum of a Bilateral and Gaussian filter.

$$\psi_p(x_i, x_j) = \mu(x_i, x_j)\left[w_1 \exp\left(\frac{|p_i - p_j|^2}{\theta_\alpha} + \frac{|I_i - I_j|^2}{\theta_\beta}\right) + w_2 \exp\left(\frac{|p_i - p_j|^2}{\theta_\gamma}\right)\right]. \quad (7)$$

Increasing θ_α, θ_β, θ_γ, w_1 and w_2 all correspond to favouring smoother predictions. The compatibility function, $\mu(x_i, x_j)$, is given by the Potts model, and is equal to 1 if $x_i \neq x_j$ and 0 otherwise [40].

Figure 13 shows the effect of varying θ_α, Fig. 14 the effect of varying θ_β and Fig. 15 the effect of varying both θ_γ and w_2. Note that in all cases, each of the other hyperparameters remains unchanged at the values from the public CRF-RNN model.

In all of these cases, we can see that increasing the smoothness does not correspond to increasing adversarial robustness to the FGSM attack. Rather, as detailed in the next subsection, there is a correlation between the confidence of the prediction and robustness to the FGSM attack.

E.2. Results about the confidence on VOC

We empirically measured the confidence of the predictions of CRF-RNN. This was done by recording the probability (from the softmax activation function) of the predicted (highest-scoring) label, and also by calculating the entropy of the marginal distribution over labels at each pixel in the image. A lower entropy indicates a more certain or confident prediction. This was then averaged over the Pascal VOC validation set.

Figures 17 and 18 show the mean confidence and entropy respectively as a function of the IoU Ratio. This is done for the FGSM attack for all the ϵ values considered in the paper. There is a clear correlation between the IoU Ratio and the confidence of the prediction. Moreover, the results of CRF-RNN are always more confident than FCN8s. Note that multiple variants of CRF-RNN, using different θ_α, θ_β and θ_γ hyperparameter values were considered, as in Figures 13 through 15.

E.3. Experiments on Deeplab v2 with CRF

In contrast to CRF-RNN [72], a common approach is to apply CRFs as a post-processing step, as done in Deeplab [15]. We perform adversarial attacks on this by appending the CRF-RNN layer of [72] onto the Deeplab v2 network. This allows us to compute the gradient of the loss with respect to the input image (required for all the attacks) by backpropagating through the CRF-RNN layer. The parameters of the CRF-RNN layer appended to Deeplab v2 were manually set to the parameters used by the original authors[10] (who obtained them via cross-validation). Note that appending the CRF-RNN layer to Deeplab v2 and using the same parameters as the authors produces output that is identical to the post-processing code used by the original authors. The difference is that this allows us to compute gradients as well.

Figures 16a and 16c show the results of targeted and untargeted attacks on Deeplab v2 with a CRF on the Pascal VOC dataset. As in the main paper, we also compute the adversarial attack from the Deeplab v2 part of the network (which produces "unaries"), and then use these perturbations to attack the entire Deeplab v2 with CRF network (Fig. 16b).

The results from these experiments are consistent with the ones of CRF-RNN in the main paper: Appending the CRF at the end of the network confers resistance to only untargeted attacks. For targeted attacks, there is barely any difference in robustness. Finally, untargeted adversarial perturbations generated from Deeplab v2, and then tested on Deeplab v2 + CRF, are actually more effective than white-box attacks on Deeplab v2 + CRF. This is due to the "gradient masking" effect of mean-field inference of CRFs which make the final prediction of the network more confident, and thus lead to gradients of the loss with respect to the input (in the untargeted case) which have smaller norm.

[10] http://liangchiehchen.com/projects/DeepLabv2_resnet.html

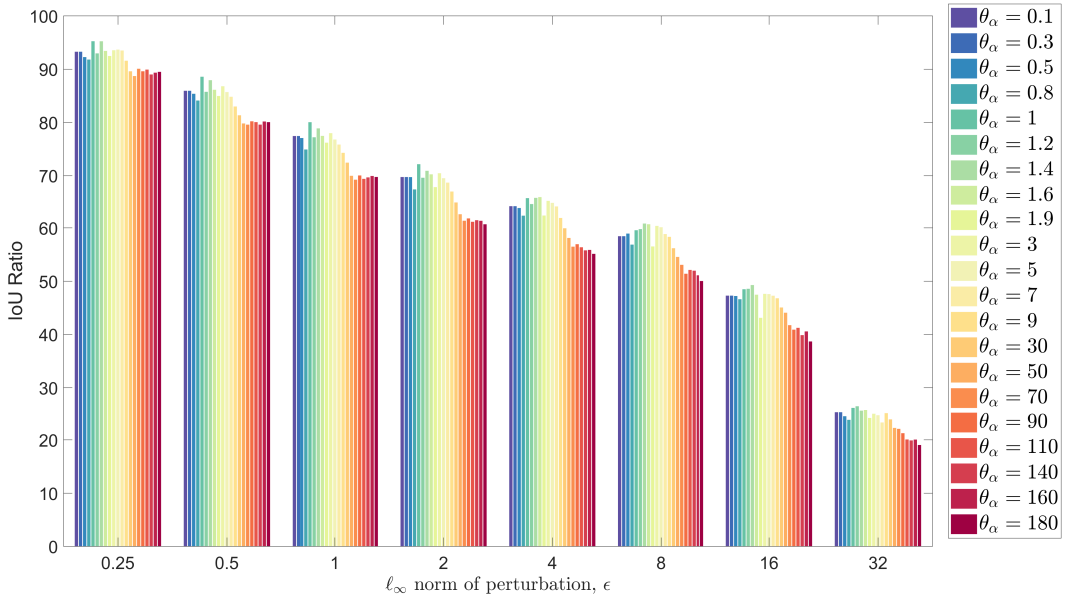

Figure 13: The IoU Ratio of CRF-RNN for various values of the θ_α (filter bandwidth) hyperparameter when attacked with FGSM on the Pascal VOC dataset. Increasing this hyperparameter visually smoothes the result further, but we can see that this does not increase adversarial robustness. In fact, lower filter bandwidths of approximately $\theta_\alpha = 1$ provide more robustness.

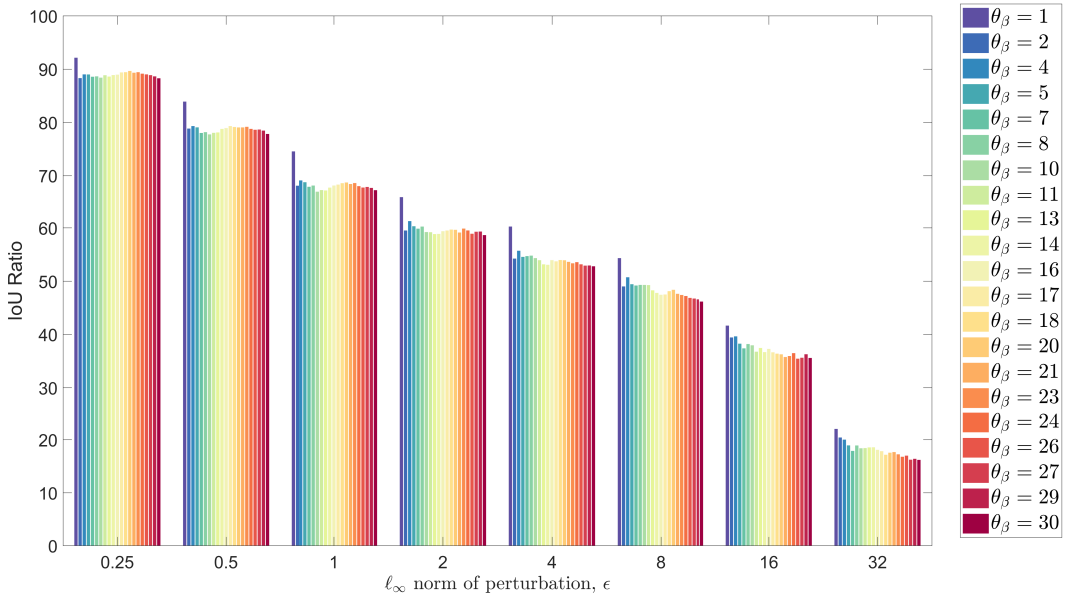

Figure 14: The IoU Ratio of CRF-RNN for various values of the θ_β (filter bandwidth) hyperparameter when attacked with FGSM on the Pascal VOC dataset. Again, we can see that larger filter bandwidths, which encourage more spatial smoothness, do not increase adversarial robustness.

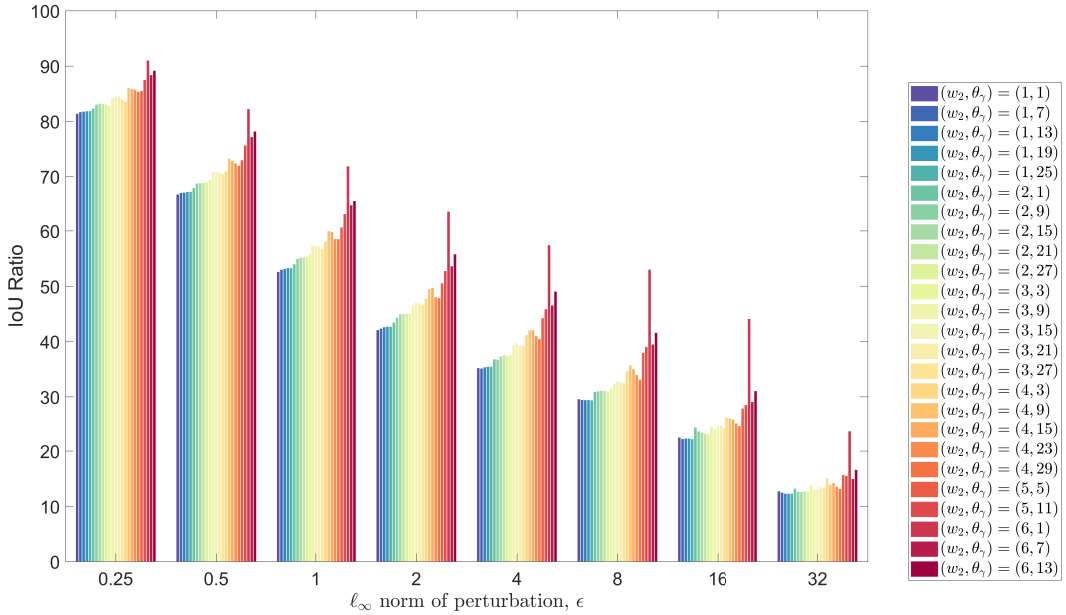

Figure 15: The IoU Ratio of CRF-RNN for various values of the w_2 and θ_γ parameters when attacked with FGSM on the Pascal VOC dataset. Increasing the weight of the Gaussian term (w_2) tends to increase robustness. However, we still see that lower filter bandwidths (θ_γ) tend to provide more robustness.

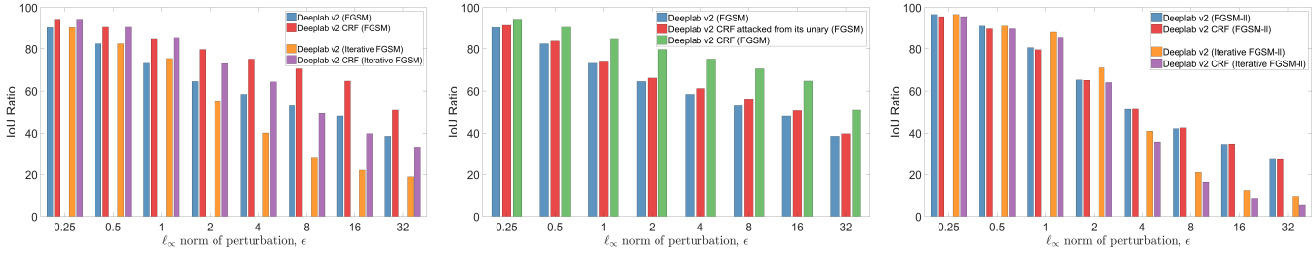

(a) (b) (c)

Figure 16: (a) On untargetted attacks, Deeplab v2 with a CRF is noticably more robust than just the Deeplab v2 network. (b) Attacks created from the base Deeplab v2 network using FGSM are more effective than those created from Deeplab v2 with CRF. This is due to the "gradient masking" effect of mean-field inference of CRFs. (c) However, the CRF does not "mask" the gradient for targeted attacks. As a result, Deeplab v2 with a CRF is no more robust than just the Deeplab v2 network.

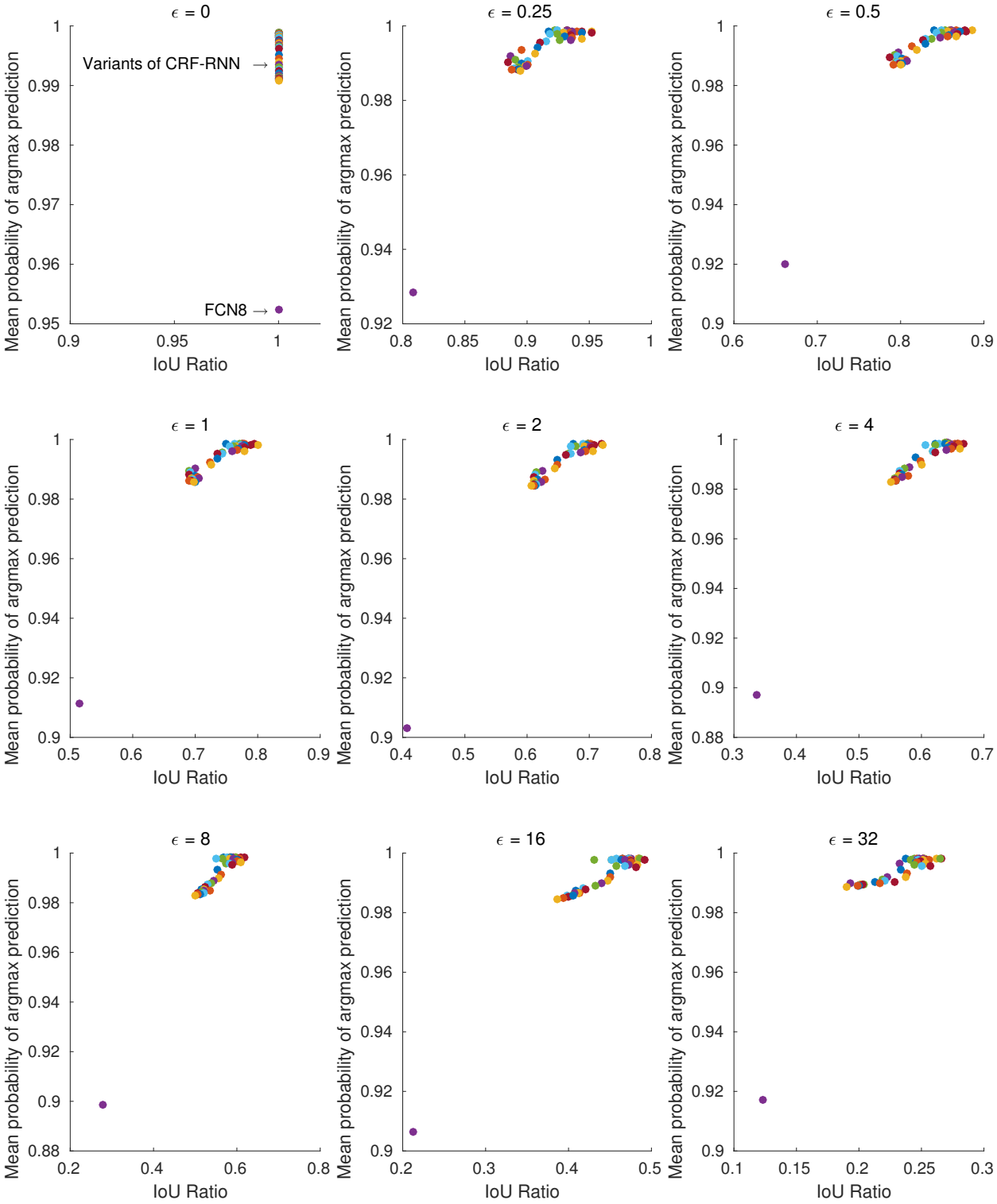

Figure 17: The mean probability of the highest-scoring class for each pixel, averaged over the Pascal VOC validation set. This is performed for the FGSM attack for multiple ϵ values. $\epsilon = 0$ corresponds to clean inputs (no adversarial attack). Note how FCN8s (the purple dot) consistently has the lowest mean probability. This probability is significantly lower than other variants of CRF-RNN (with varying θ_α, θ_β, θ_γ), shown by the other coloured dots. Moreover, note the correlation between the confidence in the prediction, and adversarial robustness to the FGSM attack. Additionally, the probability of the predicted class remains high (above 90%) for all models throughout all adversarial attacks.

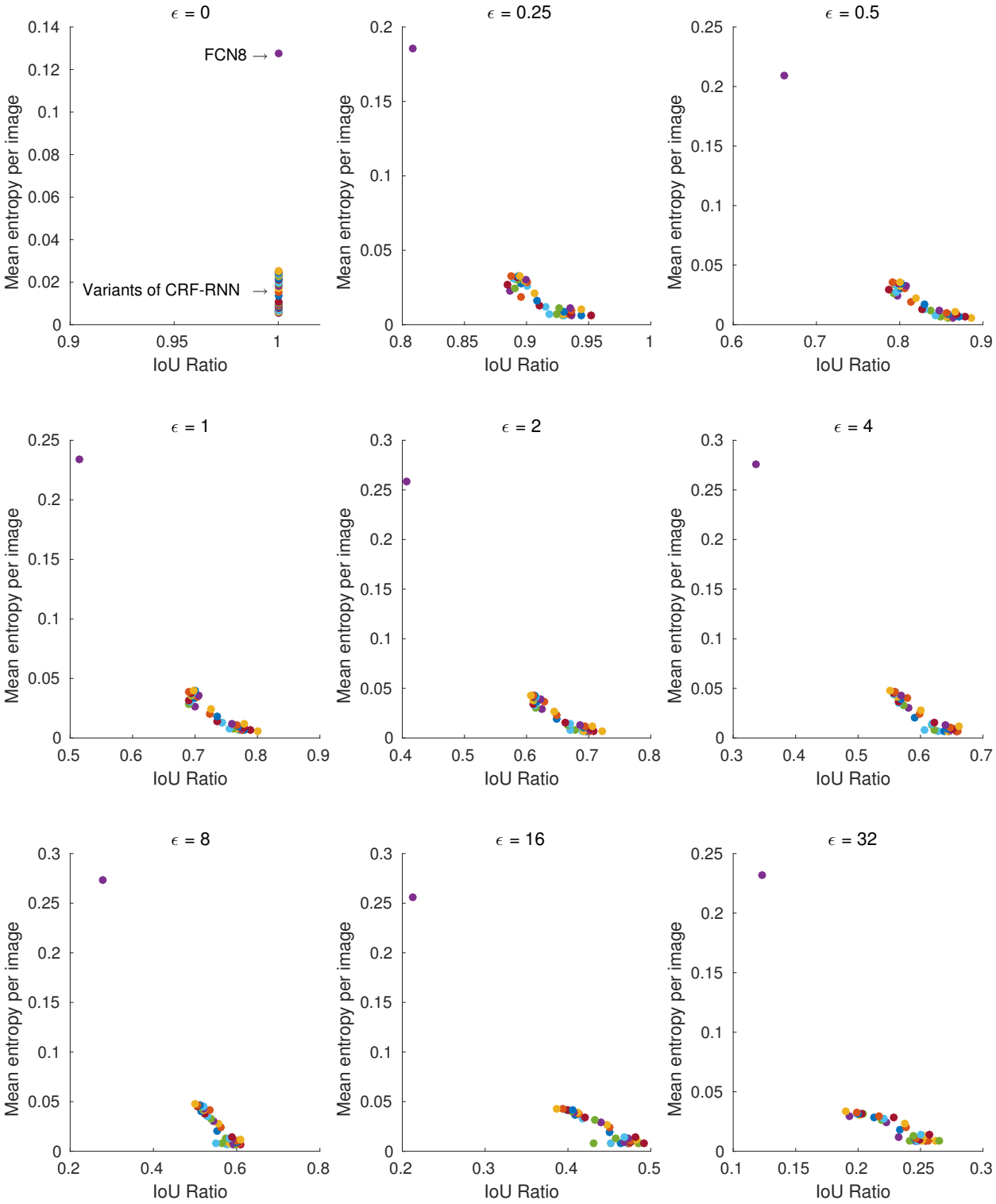

Figure 18: The mean entropy of the marginal distribution over all labels at each pixel, averaged over all images in the Pascal VOC validation set. A lower entropy corresponds to a more confident prediction. This is performed for the FGSM attack for multiple ϵ values. $\epsilon = 0$ corresponds to clean inputs (no adversarial attack). Note how FCN8s (the purple dot) consistently has the highest mean entropy (least confidence). This entropy is significantly higher than other variants of CRF-RNN (with varying θ_α, θ_β, θ_γ), shown by the other coloured dots. Moreover, note the correlation between the confidence in the prediction, and adversarial robustness to the FGSM attack.